Chapter 2
Fundamentals

Any sufficiently advanced technology is indistinguishable from magic.

—Arthur C. Clark

This chapter will give an introduction to the fundamental physics and processes, which are necessary to understand the present work. It will start with an overview of the properties of organic semiconductors followed by some basics of electronic structure theory. Subsequently, different models and processes relevant for interfacial energy–level alignment will be discussed.

2.1 Organic Semiconductors: π–Conjugated Molecules

Organic molecules are the multitude of compounds of carbon (covalently) bound to itself or other elements. Typical other atoms are hydrogen, oxygen, nitrogen, sulfur or fluorine. Since carbon can participate in up to four unpolar bonds to other carbons, iteration to large molecules is possible and common (e.g., the DNA). Therefore, a wealth of organic compounds is known. Yet, central to this work are organic semiconductor (OSC), which usually refers to the subgroup of organic molecules that have a π–conjugated (electron) system. Such a π–conjugated system consists of delocalized electrons from former p–orbitals, which are described in the limits of alternating single and double bonds. The conjugation of the bonds enforces that OSCs are, at least in parts, planar. The origin of this behavior is to find in the sp^2 hybridization of carbon.

Here, hybridization refers to linear combinations of the carbon's 2 s and 2p atomic orbitals, which best describe the experimentally observed bonding modalities. E.g., often one finds carbon tetrahedrally coordinated exhibiting four equivalent bonds. This configuration is described by sp^3 hybridization. The relevant case for π–systems, though, is sp^2 hybridization. In sp^2 hybridization only two of the three 2p orbitals mix with the 2 s orbital yielding three equivalent sp^2 hybrid orbitals.

© Springer International Publishing AG 2017

R. Schlesinger, *Energy-Level Control at Hybrid Inorganic/Organic Semiconductor Interfaces*, Springer Theses, DOI 10.1007/978-3-319-46624-8_2

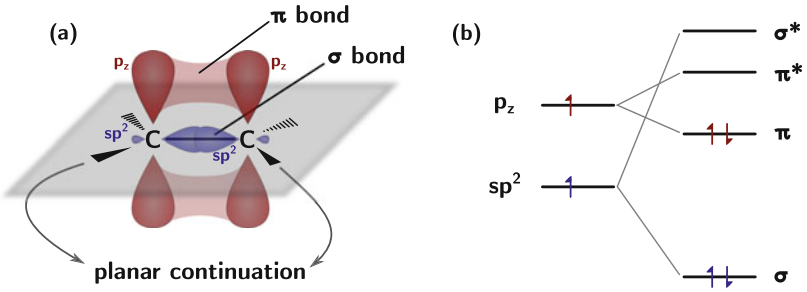


Fig. 2.1 **a** Scheme of the covalent bonding between two sp^2 hybridizated carbon atoms. Each of the carbons has three hybrid sp^2 orbitals (*black* markers) lying in a common plane (*grey*). The p_z orbital is perpendicular to the three sp^2 hybrid orbitals. Upon bond formation two sp^2 hybrids form a σ bond (orbitals indicated in the plane). The overlap between the two p_z orbitals mediates a π–bond. To maximize the π–bond overlap the p_z orbitals favor to align parallel. At the same time this forces the sp^2 hybrids of both carbons into a common plane (*grey*). Therefore, molecules containing carbons in sp^2 hybridization tend to be planar, at least in parts. **b** Due to the different overlap of the sp^2 and p_z orbitals, the energy levels of σ orbitals are usually stronger split than those of the π orbitals. Thus, HOMO and LUMO of OSCs are usually π orbitals. σ^* and π^* denote the unoccupied, antibonding, states of the situation depicted in **a**

They are directed in a common plane, rotated by 120° each. The fourth orbital, the remaining p_z, is directed normal to that plane. If now sp^2 hybridized constituents bond, their atomic nuclei are usually arranged in a single common plane, which is that of the sp^2 hybrids. This can be understood by the scheme in Fig. 2.1. Upon bonding of two neighboring sp^2 hybridized constituents two of their sp^2 orbitals form a σ–bond (rotationally symmetric along the bond axis). Additionally, a π–bond is formed due to the overlap between the adjacent p_z orbitals. To maximize the overlap of the π–bond the p_z orbitals have to align parallel, forcing all sp^2 hybrid orbitals in the very same plane. Note that there exist exceptions from this rule. E.g., in para–sexiphenyl the repulsion between (terminal) hydrogen atoms induces a twisting between the neighboring phenyl ring units.

Since the overlap of the p_z orbitals is usually smaller than that of the sp^2 hybrids, the energy level splitting of the p_z states is also less (see Fig. 2.1b). Thus, the important electrical transport states, i.e., the highest occupied molecular orbital (HOMO) and the lowest unoccupied molecular orbital (LUMO), are π–states. Those states are responsible for many of the typical properties of organic semiconductors. The energies of the π–states can approximately be calculated via the Hückel method, which is described in Sect. 2.2.2.1. By changing the overlap within the π–system or changing its electron density, e.g., by electron withdrawing or donating side groups, one can modify the π–system's energy levels. This opens up vast possibilties to design molecules for a particular purpose by exploiting the versatility of chemical synthesis and side group engineering.

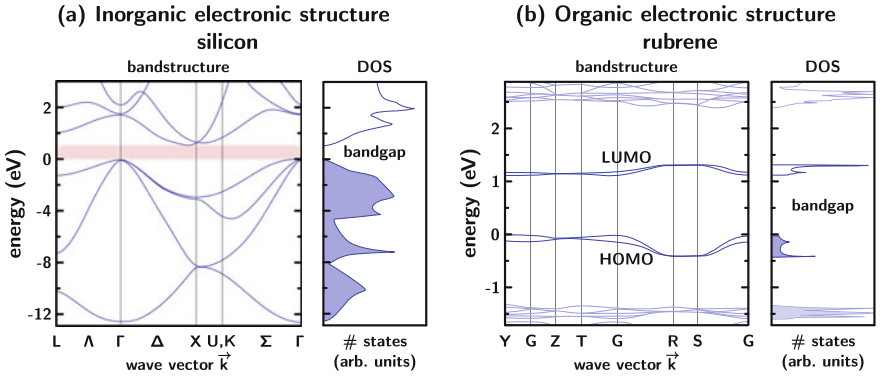


Fig. 2.2 Typical electronic structures exemplified by **a** Si and **b** rubrene. Shown are calculated bandstructures along high symmetry axes of the brillouin zone and the resulting DOS. For Si the bandgap (blurred region) is indirect. One can see that the Si valence bands along LΛΓ and ΓΔX are almost degenerate, but split along KΣΓ. Their bandwidths are several eV. **b** Organic semicondcutors usually exhibit far smaller dispersions than inorganic semiconductors. Here the bandwidth of the HOMO and LUMO is below 0.4 eV. Note the different energy scale than in **a**. As it will be discussed in the text not every point of zero slope (van Hove singularity) of the band structure leads to a divergent DOS. Graphs are adapted from [2, 3]

Due to the closed shell nature of OSC molecules the intermolecular forces are generally weak and of van der Waals type. This type of interaction can well be described by the Lennard–Jones potential [1]:

$$V(r) = 4V_0 \left[\left(\frac{d_{\text{eff}}}{r} \right)^{12} - \left(\frac{d_{\text{eff}}}{r} \right)^{6} \right] \tag{2.1}$$

here the first term empirically describes the Pauli repulsion between the molecules, which is a consequence of the exchange interaction of Fermions. Sometimes, alternatively, an exponential functional form is used for the first term. The second term describes the interaction of fluctuating mutually induced dipoles (which exists even for neutral molecules). It is thus linked with the polarizabilities, which in turn, for OSCs, are dominated by the π–system. Due to the weaker intermolecular forces, OSC crystals are softer and not as thermally stable as their inorganic counterparts. For the same reason the bandstructures of inorganic and organic crystals are also markedly different: Due to the stronger interaction of inorganic semiconductors their bandstrutures are characterized by stronger band dispersion and larger bandwidths of several eV. In contrast, a molecular crystal of rubrene only exhibits weak dispersion and a maximum bandwidth of only 0.4 eV. Noteworthy, rubrene is a benchmark molecular crystal. Hence, other OSCs usually exhibit even weaker dispersion. Thus, the bandstructures of molecular crystals indeed mostly resemble just the molecular energy levels (Fig. 2.2).

Another difference of inorganic semiconductors and OSCs concerns the excitons. On the one hand, in inorganic semiconductors the mean distances of excitons are large and hence binding energies low. Such excitons are called Wannier excitons. Indeed, the exciton binding energy of ZnO (60 meV) is among the highest to find for inorganic semiconductors. On the other hand, for OSCs, positive and negative charge of the exciton are close usually confined within the boundaries of the same (small) OSC molecule. Such excitons are called Frenkel excitons. Furthermore, due to the presence of the exciton, the molecules adjust/relax themselves (nuclei and electrons) to establish a new lowest energy conformation. The relaxation energies are regularly in the range of a few 100 meV. Thus, Frenkel excitons exhibit significantly stronger binding energies than Wannier excitons.

Similarly, also an additional charge carrier induces a relaxation of the molecule it resides on. Thus, the binding energy of such a polaron is also of the order of a few 100 eV, which severely hinders its charge transport. Consequently, the highest observed mobilities for OSC crystals, e.g., rubrene, only reach 20 cm^2/Vs [4]. This is by far below typical values found for inorganic semiconductor crystals (e.g., GaAs $\mu > 9000\,cm^2$/Vs [5]). The charge transport in OSCs is usually best describes by hoppping transport models, in which intersite hopping occurs through tunneling and is temperature activated [6–9]. In contrast most inorganic semiconductors exhibit bandlike transport, in which mobilities $q \langle \tau \rangle / m^*$ depend on the mean scattering time $\langle \tau \rangle$ of the charge carriers [10, p. 207]. Also the temperature dependence is different. For instance, different than in hopping transport, raising the temperature in the band transport regime lowers the mobility, since phonon scattering is enhanced (not considering ionized impurity scattering). For a thorough discussion of the temperature dependencies of the mobilities in the band and hopping transport regimes see, e.g., [10, 11, p. 220]. Lastly, for OSCs, the hopping matrix elements are dependent on the $(\pi - \pi)$ overlap and therefore charge transport is commonly anisotropic. As an example: The charge transport will be different depending on whether molecules are lying face–on or standing on the heterointerfaces of a (planar) device. Note that different interfacial molecular orientations are observed at several instances within this work.

2.2 Electronic Structure Theory

Now some of the fundamental concepts and terms of solid state electronic structure theory will be introduced. The discussion starts with aspects of strictly periodic structures, which are best applicable to inorganic semiconductors. Nevertheless, this is also relevant to the understanding of organic semiconductors, since first, organic semiconductors can also form crystals and second, both fields share many terminologies. Focus is put on two limits of how to calculate band structures: the nearly free electron and the tight binding approximation. The latter, the tight binding model, is particularly valuable for the field of organic semiconductors, since it is applicable to

non–periodic structures. Its application to organic semiconductors in the variant of the Hückel method is also presented.

One often finds matter to be organized in periodic structures so that atoms or molecules are at defined positions on a lattice. This has numerous consequences for the electronic structure. E.g., simply by considering a periodic potential of delta functions, i.e., the Kronig–Penney model, one can already explain the existence of bands. More advanced discussions of electronic structure need to consider more realistic potentials and usually start from the single particle Schrödinger equation, in which electron–electron interactions of the form $V(\vec{r}_\mathrm{i} - \vec{r}_\mathrm{j})$ are excluded:

$$\hat{\boldsymbol{H}}\,\psi\,(\vec{r}) = \left(-\frac{\hbar^2}{2m}\Delta + V\,(\vec{r})\right)\psi\,(\vec{r}) = E\,\psi\,(\vec{r}) \tag{2.2}$$

where $V(\vec{r}) = V(\vec{r} + \vec{R})$ is the periodic crystal potential, which is invariant upon translations by Bravais vectors $\vec{R}$. Note that vectors are denoted by an arrow above and quantum mechanic operators, e.g., the Hamilton operator $\hat{\boldsymbol{H}}$, in boldface with a hat. The periodicity of the crystal also forces the wavefunctions ψ in different unit cells to differ by only a phase factor. By this the electron density $|\psi|^2$ is fully periodic over the unit cells, which is known as Bloch's theorem:

$$\psi_{\vec{k}}(\vec{r}) = e^{i\vec{k}\cdot\vec{r}} \cdot u(\vec{r}) \qquad u(\vec{r}) = u(\vec{r} + \vec{R}) \tag{2.3}$$

where $u(\vec{r})$ is a lattice periodic function. The solutions to the Schrödinger equation can be indexed by their wave vector. However, it is common to restrict $\vec{k}$ to the first Brillouin zone and construct values outside by appropriate addition / subtraction of reciprocal lattice vectors $\vec{G}$. Within this reduced zone scheme one needs a second index to differentiate between the now multiple solutions for a single $\vec{k}$. That is the band index, which is either labeled n or by the reciprocal lattice vector $\vec{G}_\mathrm{n}$.

2.2.1 Nearly Free Electrons

Using the introduced formalism of reciprocal lattice vectors one obtains the Fourier transformed Schrödinger equation as:

$$\left[\frac{\hbar^2}{2m}\left(\vec{k} - \vec{G}_\mathrm{n}\right)^2 - E\right] c_{\vec{k}-\vec{G}_\mathrm{n}} + \sum_{\vec{G}} V_{\vec{G}-\vec{G}_\mathrm{n}} c_{\vec{k}-\vec{G}} = 0 \tag{2.4}$$

where $c_{\vec{k}-\vec{G}_\mathrm{n}}$ and $V_{\vec{G}-\vec{G}_\mathrm{n}}$ are the Fourier coefficients of the expanded wavefunction ψ and of the potential V respectively. From this equation one can recognize that the dispersion upon neglecting the potential (all $V_{\vec{G}-\vec{G}_\mathrm{n}} = 0$) resembles the one of free electrons, indexed by bands:

$$E_{\mathrm{n}}^{(0)}(\vec{k}) = E_{\vec{k}-\vec{G}_{\mathrm{n}}}^{(0)} = \frac{\hbar^2}{2m}\left(\vec{k} - \vec{G}_{\mathrm{n}}\right)^2 \tag{2.5}$$

However, neglecting the crystal potential is not very realistic, since at least a small potential will always be present. In this case one utilizes second order perturbation theory in the small potential. Starting from (2.4) one obtains the Brillouin–Wigner perturbation series [12, p. 103] for the energy dispersion $E_{\mathrm{n}}(\vec{k})$:

$$E_{\mathrm{n}}(\vec{k}) = E_{\vec{k}-\vec{G}_{\mathrm{n}}}^{(0)} + \sum_{\vec{G}\neq\vec{G}_{\mathrm{n}}} \frac{\left|V_{\vec{G}-\vec{G}_0}\right|^2}{E_{\mathrm{n}}(\vec{k}) - E_{\vec{k}-\vec{G}}^{(0)}} \tag{2.6}$$

It is evident that the energies $E_{\mathrm{n}}(\vec{k})$ deviate from the undisturbed energies $E_{\vec{k}-\vec{G}_{\mathrm{n}}}^{(0)}$ of free electrons upon switching on a potential. By approximating $E_{\mathrm{n}}(\vec{k})$ in the denominator by $E_{\vec{k}-\vec{G}_{\mathrm{n}}}^{(0)}$, Eq. (2.6) becomes the 2nd order Rayleigh–Schrödinger perturbation series. However, the Rayleigh–Schrödinger series connot be used at critical points $\vec{k}$, for which $E_{\vec{k}_{\mathrm{crit}}-\vec{G}_{\mathrm{i}}}^{(0)} = E_{\vec{k}_{\mathrm{crit}}-\vec{G}_{\mathrm{n}}}^{(0)}$, since there the denominator is zero. This occurs at points of the first Brillouin zone, where two bands are degenerate (cross). Such is often fulfilled at the zone boundaries. By separating out the critical summand in (2.6) one obtains a quadratic relation for $E_{\mathrm{n}}(\vec{k}_{\mathrm{crit}})$ and calculates the resulting band splitting at the points $\vec{k}_{\mathrm{crit}}$ approximately as [12, p. 103]:

$$E_{\mathrm{crit}}^{\pm}(\vec{k}) = E^{\pm}(\vec{k}_{\mathrm{crit}}) = E_{\vec{k}_{\mathrm{crit}}-\vec{G}_{\mathrm{n}}}^{(0)} \pm \left|V_{\vec{G}_{\mathrm{n}}-\vec{G}_{\mathrm{i}}}\right| \tag{2.7}$$

One can use Eq. (2.7) to estimate the size of the bandgap as two times the (first) Fourier coefficient. One should note that this is only an approximation and bands can stay degenerate, meaning that they do not need to split.

2.2.2 Model of Tight Binding/LCAO

Within the just presented nearly free electron approximation one can understand the occurrence of bands as an intrinsic consequence of a periodic potential. While this approximation might be good for certain systems (e.g., metal conduction electrons), many electrons of a crystal can not be considered nearly free. Thus, now the opposite approach is discussed. It considers electrons to be strongly bound to the atomic nuclei, which is called tight binding (TB). To reflect this new notion one rewrites the Hamiltonian for a single electron in the following form:

$$\hat{\boldsymbol{H}} = \frac{\hat{\boldsymbol{p}}^2}{2m} + \sum_{\vec{R}_{\mathrm{i}}} V_{\mathrm{at}}(\vec{r} - \vec{R}_{\mathrm{i}}) \tag{2.8}$$

$$= \left(\frac{\hat{\boldsymbol{p}}^2}{2m} + V_{\text{at}}(\vec{r} - \vec{R}_{\text{x}}) \right) + \sum_{\vec{R}_{\text{i}} \neq \vec{R}_{\text{x}}} V_{\text{at}}(\vec{r} - \vec{R}_{\text{i}}) \tag{2.9}$$

$$= \hat{\boldsymbol{H}}_{\text{at},\vec{R}_{\text{x}}} + \hat{\boldsymbol{H}}_{\text{ext}} \tag{2.10}$$

which is still the same single particle Hamiltonian as in (2.2). One recognizes the atomic Hamiltonian of a single atom at $\vec{R}_{\text{x}}$ to be disturbed by the potential of the other atomic nuclei's potentials $V_{\text{at}}(\vec{r} - \vec{R}_{\text{i}})$ at positions $\vec{R}_{\text{i}}$. Note that the $\vec{R}_{\text{i}}$ are not necessarily periodic, which predestines the approach to be used for organic semiconductors as well.

Since within tight binding electrons are strongly bound, one can use the atomic orbitals $\phi_{\text{n}}(\vec{r} - \vec{R}_{\text{i}})$ as an approximation to the wavefunctions. Furthermore, in the periodic lattice of a crystal the wavefunctions have to be normalized[1] and fulfill Bloch's theorem. Accordingly, one constructs wavefunctions from the atomic orbitals $\phi_{\text{n}}(\vec{r} - \vec{R}_{\text{i}})$ as a linear combination of atomic orbitals (LCAO):

$$\psi_{\text{n}\vec{k}}(\vec{r}) = \frac{1}{\sqrt{N}} \sum_{\vec{R}_{\text{i}}} e^{i\vec{k}\vec{R}_{\text{i}}} \phi_{\text{n}}(\vec{r} - \vec{R}_{\text{i}}) \tag{2.11}$$

With these wavefunctions one uses (2.12) to calculate the band energies, i.e., the dispersion relations:

$$E_{\text{n}}(\vec{k}) = \frac{\langle \psi_{\text{n}\vec{k}} | \, \hat{\boldsymbol{H}} \, | \psi_{\text{n}\vec{k}} \rangle}{\langle \psi_{\text{n}\vec{k}} | \, \psi_{\text{n}\vec{k}} \rangle} \tag{2.12}$$

In calculating the matrixelements in (2.12) (cf. also (2.14)–(2.16)) one exploits that $\phi_{\text{n}}, \phi_{\text{n}}^*$ and V_{at} are localized functions around a single atomic site but small everywhere else. If neglecting terms, in which all three are small, one obtains the following dispersion relations using only the relevant:

$$E_{\text{n}}(\vec{k}) = E_{\text{n}} + \frac{\beta_{\text{n}} + \sum_{\vec{R}_{\text{i}} \neq 0} e^{-i\vec{k}\vec{R}_{\text{i}}} \lambda_{\text{n}}(\vec{R}_{\text{i}})}{1 + \sum_{\vec{R}_{\text{i}} \neq 0} e^{-i\vec{k}\vec{R}_{\text{i}}} \alpha_{\text{n}}(\vec{R}_{\text{i}})} \tag{2.13}$$

This equation uses the abbreviations (2.14)–(2.16), for the non–neglected matrix-elements. Here β is the atomic energy shift due to the potential of the neighboring atoms, λ the inter atomic matrix element and α the overlap integral:

[1] For reasons of simplicity the wavefunction of (2.11) are not orthonormal, which is not problematic, since energies will be calculated via the Ritz method (2.12) anyway.

$$\beta_{\mathrm{n}} = \int d^3r\, \phi_{\mathrm{n}}^*(\vec{r}) \sum_{\vec{R}_{\mathrm{i}} \neq 0} V_{\mathrm{at}}(\vec{r} - \vec{R}_{\mathrm{i}})\, \phi_{\mathrm{n}}(\vec{r}) \tag{2.14}$$

$$\lambda_{\mathrm{n}}(\vec{R}_{\mathrm{i}}) = \int d^3r\, \phi_{\mathrm{n}}^*(\vec{r} - \vec{R}_{\mathrm{i}})\, V_{\mathrm{at}}(\vec{r} - \vec{R}_{\mathrm{i}})\, \phi_{\mathrm{n}}(\vec{r}) \tag{2.15}$$

$$\alpha_{\mathrm{n}}(\vec{R}_{\mathrm{i}}) = \int d^3r\, \phi_{\mathrm{n}}^*(\vec{r} - \vec{R}_{\mathrm{i}})\, \phi_{\mathrm{n}}(\vec{r}) \tag{2.16}$$

It is common to restrict the summations in (2.13) to a few nearest neighbor interactions. E.g., a 3D simple cubic lattice in next neighbor approximation leads to three cosine terms in the different directions of space and thus a bandwidth of $12\,\lambda$:

$$E(\vec{k}) = E_0 - 2t\left[\cos(k_{\mathrm{x}}a) + \cos(k_{\mathrm{y}}a) + \cos(k_{\mathrm{z}}a)\right] \tag{2.17}$$

The wavefunctions (2.11) used were constructed from only one atomic wavefunction ϕ_n from each site. But this way constructed wavefunctions are not eigenfunctions of the tight binding Hamiltonian. In order to circumvent this problem, a better ansatz is to expand the wavefunction in the Hilbert space of all atomic orbitals. This variant of a LCAO (as opposed to (2.11)) advances the ansatz of (2.11) to now include mixing of different wavefunctions, e.g., s with p or d.

2.2.2.1 The Hückel Method

The Hückel method or also the Hückel molecular orbital method (HMO) is a special case of the tight binding approximation to calculate the energy levels (and orbitals) of the π–states of organic semiconductors. This is possible, since periodicity is not necessarily required in the tight binding ansatz. The interesting electronic π–states of conjugated organic molecules are mainly derived from the p_{z} orbitals of the carbon backbone atoms. Consequently, all π bonds are indeed equivalent (benzene) or at least close to it (larger conjugated molecules). Therefore, the Hückel method uses the LCAO approach to construct the π–state wavefunctions from the atomic p_{z} orbitals as:

$$|\psi\rangle = c_1\,|\phi_1\rangle + c_2\,|\phi_2\rangle + \cdots + c_{\mathrm{N}}\,|\phi_{\mathrm{N}}\rangle \tag{2.18}$$

where N refers to the indexing of the atomic constituents of the π–system. Here constituents mean that hydrogen atoms or parts of the molecules, e.g., spiro groups, are excluded, which do not contribute electrons to the π–system. Substituting (2.18) in the Schrödinger equation (2.10) and multiplying the ket vectors $|\phi_{\mathrm{j}}\rangle$ with the corresponding bra vectors $\langle\phi_{\mathrm{i}}|$ one obtains the following system of Eqs. (2.19):

$$\begin{array}{l}(H_{11} - S_{11}E)\,c_1 + (H_{12} - S_{12}E)\,c_2 + \cdots + (H_{1N} - S_{1N}E)\,c_N = 0\\ (H_{21} - S_{21}E)\,c_1 + (H_{22} - S_{22}E)\,c_2 + \cdots + (H_{2N} - S_{2N}E)\,c_N = 0\\ \qquad\vdots \qquad\qquad\qquad\qquad\qquad\qquad\qquad\qquad\vdots\\ (H_{N1} - S_{N1}E)\,c_1 + (H_{N2} - S_{N2}E)\,c_2 + \cdots + (H_{NN} - S_{NN}E)\,c_N = 0\end{array} \tag{2.19}$$

$$H_{ij} = \langle\phi_i|\,\hat{\boldsymbol{H}}\,|\phi_j\rangle \qquad S_{ij} = \langle\phi_i\,|\phi_j\rangle \tag{2.20}$$

Here, S_{ij} are the overlap integrals. The diagonal matrixelements H_{ii} are called coulomb integrals and the off diagonal ones (H_{ij}) resonance integrals. The Hückel approximation (see (2.21)) now consists of three assumptions on these integrals: First, it assumes that any overlap between neighboring atoms vanishes. Second, one assumes all coulomb integrals to be equal. Third, only resonance integrals of next neighbors are non–vanishing and all of them are equal [13–16]:

$$S_{ij} = \delta_{ij} \qquad H_{ii} = \alpha \qquad H_{ij}^{adjacent} = \beta \tag{2.21}$$

Using these approximations and solving the system of linear equations (2.19) for nontrivial solutions one obtains the determinant (2.22).[2] Having used the Hückel approximation the solution of the determinant (2.22) is now much simpler. Finding the energy eigenvalues is now a FindRoot problem of the same polynomial order as there are carbon/constituent atoms in the π—system. It can even be done "by hand" for academic examples as benzene.

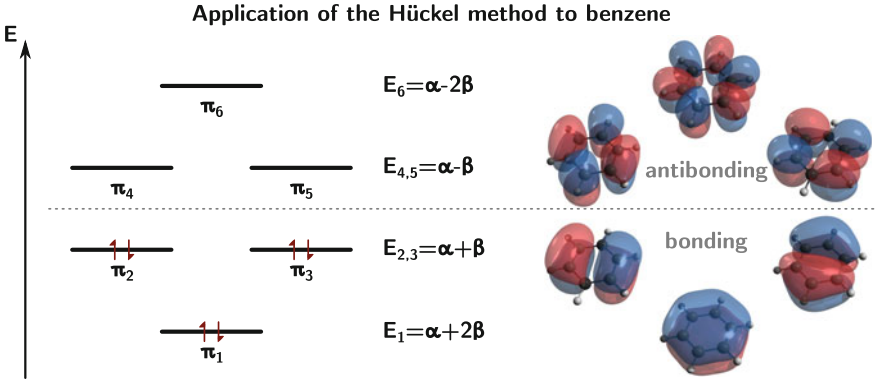


Fig. 2.3 π–Orbital energies of benzene calculated via the Hückel method. HOMO and LUMO are both twofold degenerate. To the right renderings of the corresponding π–orbitals' isosurfaces are shown. One realizes that bonding (antibonding) orbitals also have nodal planes (lobes) between selected atoms leading to repulsive (attractive) interaction. Thus, the terms bonding and antibonding orbitals must be used carefully

[2]Note that the β's in the top right and bottom left cell of the determinant in (2.22) are only present for a cyclic molecule, since, e.g., in benzene the first and sixth carbon atom are adjacent.

$$\begin{vmatrix} \alpha - E & \beta & 0 & \dots & \beta \\ \beta & \alpha - E & \beta & \dots & 0 \\ 0 & \beta & \alpha - E & \dots & 0 \\ \vdots & \vdots & \vdots & \dots & \vdots \\ \beta & 0 & 0 & \dots & \alpha - E \end{vmatrix} = 0 \tag{2.22}$$

By the Hückel method it is simple to gain an understanding of how many π–states there are, which of them are degenerate and also how the corresponding wavefunctions look like. This will now be illustrated by applying the Hückel method to benzene: For benzene equation (2.22) has six roots, of which two are pairwise degenerate (see Fig. 2.3). Note that β is negative so that for instance the energy of the HOMO is $\alpha+\beta$. To the right hand side of Fig. 2.3 the corresponding orbitals are shown. This picture can easily be obtained within the Hückel method by inspecting the phases of the individual p_z orbitals contributing to the wavefunction. Such a figure is instructive, since it visualizes the bonding modalities via the lobes and nodes of the wavefunctions. Note that the unoccupied states are commonly called antibonding. However, from inspection of Fig. 2.3 it becomes clear that also antibonding orbitals can be attractive between selected atoms and vice versa also bonding orbitals repulsive.

2.2.3 *The Density of States*

The energy of an electron in a solid is linked with its wave vector k via the dispersion relation (bandstructure). In many cases, though, one is not interested in the dispersion relation, but rather in how many states exist at a certain energy. This quantity is the density of states (DOS). Within the scope of this work the DOS will be used on several occasions and mostly phenomenologically. Nevertheless, it will now be shown how the bandstructure and DOS are related. Furthermore, the functional form of the DOS at semiconductor band edges will be derived.

The most general form to calculate the DOS is of course simply counting the states within an energy interval $(E, E+\delta E)$. But with the dispersion relation $E(\vec{k})$ known, one can calculate the density of states $g(E)$ by the surface integral (in k space) over areas A of constant energy E [17, p. 144]:

$$g(E) = \int_A \frac{dA}{4\pi^3} \frac{1}{|\vec{\nabla}_k E(\vec{k})|} \tag{2.23}$$

Unfortunately, the precise form of those equi–energy surfaces or the bandstructure in general can be quite complex. Thus, Eq. (2.23) still poses a severe hurdle for calculating the DOS. The only remedy is to use locally (approximated) functional forms for $E(\vec{k})$, so that evaluation of (2.23) is easy, or fall back to a numerical treatment. It is clear that integration in (2.23) over points for which $|\vec{\nabla}_k E(\vec{k})| = 0$ is critical. These points are called van Hove singularities. Notably, the DOS at such

points does not necessarily diverge, but can. Since $E(\vec{k})$ is a periodic function on the reciprocal lattice, there indeed exist points in every band, where the gradient vanishes.[3] Two prominent points, for which $|\vec{\nabla}_k E(\vec{k})| = 0$, are the band edges of conduction and valence band.

To calculate the DOS around the conduction and valence band edges one can parabolically approximate the dispersion relation $E(\vec{k}) = \frac{\hbar^2 k^2}{2m^*}$, using the effective mass m^*. Then, surfaces of equal energy in (2.23) are spheres and evaluation of (2.23) yields:

$$g_C(E) = \frac{(2m_e^*)^{\frac{3}{2}}}{2\pi^2\hbar^3}\sqrt{E - E_C} \qquad g_V(E) = \frac{(2m_p^*)^{\frac{3}{2}}}{2\pi^2\hbar^3}\sqrt{E_V - E} \tag{2.24}$$

for the DOS of the conduction ($[g_C(E)]$) and valence band ($g_V(E)$) relative to the band edges E_C and E_V. m_e^* and m_p^* are the electron and hole effective masses, which are usually not equal. From (2.24) one realizes that the DOS at the extremal points at the band edges stays finite, even zero.

Note the typical $\sim\sqrt{E}$ form of a 3D system. Differently dimensional systems, e.g., a 2D electron gas, usually exhibit a different functional form. Lastly, it should be mentioned that certain letters put in front of the term DOS refine its meaning. That way LDOS or JDOS refer to the local DOS or joint DOS.[4] Most importantly GDOS will be used to name the gap state density of states within this thesis.

2.2.4 Gap States

For many discussions of electrical properties or energy–level alignment, it is sufficient to know the positions of the bands (or molecular states) and the forbidden energy regions in between, i.e., the bandgaps. However, a problem with this simple picture arises if the bandgap is not completely empty, but houses states itself. These gap states are of paramount importance for energy–level alignment, since they are close to E_F. Therefore, their occupation sensitively responds to any change of the energy–level alignment and vice versa.

There exist several origins, which can give rise to states within the bandgap. Many of those origins exclusively occur at surfaces or interfaces. The present thesis will subsummize all states in the gap, possibly having different physical origins, under the phenomenological term "gap states". For discussing energy–level alignment using such a general term is not an issue, since it is primarily important that there exist DOS in the gap, but not what is its origin. Also, in many cases it is experimentally impossible to pinpoint the particular physical cause for a gap state, so that a general term is required. Yet, for the discussion of other physical properties it can be important to know the origin of a gap state. E.g., the wavefunctions of the various

[3] Not considering special cases as discontinuous $E(\vec{k})$ relations.

[4] Which is the product of initial and final densities used to count, e.g., transition states.

types of gap states can be differently localized/extended, which is interrelated with the conductance of the material or across an interface. Therefore, some origins of gap states shall be discussed in more detail:

A probably not complete list of terms used in relation with gap states is: surface states (Shockley and Tamm states) [18, 19], interface states, metal induced gap states (MIGS) [19], Urbach tails [20–22] and (electron) band tails [23–25]. Surface states are, as the name suggest, states that occur at and due to the surface. Depending on the mathematical treatment, they are classified as Shockley or Tamm states. Interface states is a general term for states existing only confined at an interface. Noteworthy, by these definitions one could also consider a surface state (or a MIGS) an interface state. MIGS refer to a behavior, which is not necessarily specific for metals: The energy of a state on one side of an interface is usually[5] met by a forbidden energy region on the other side of an interface. But even though the energy of the state on one side is forbidden on the other, its wavefunction does not abruptly vanish on the other side, but decays exponentially with distance from the interface. Hereby, states which are strictly allowed only on one side, also become interface confined gap states of the other side. Note that this is similar to the induced density of interface states (IDIS). Finally, the term Urbach tails refers to exponential tailing of the absorption edge in optical spectroscopy, which is related to disorder in the material. While strictly speaken Urbach tails are connected with the JDOS their mathematical treatment is intertwined with the more general topic of disorder induced electron band tails. Particularly the latter two, Urbach and electron band tails, can also be bulk properties, while the others are surface/interface confined.

From all those possible origins only surface states and electron band tails are necessary to be further discussed (see Sects. 2.2.4.1 and 2.2.4.2). Surface states are discussed mainly for academic reasons (Sect. 2.2.4.1), since for them it can be easily shown that the states exist in the bandgap. Additionally, a short excerpt about electron band tails is necessary to understand the GDOS investigations of Sect. 5.3.

2.2.4.1 Surface States

In 1932 Tamm's pioneering work [26] paved the way for the field of surface states as a direct consequence of terminating a crystal with a surface. Similarly important is the work of Shockley, who treated surface states in the framework of nearly free electrons. Except for the nomenclatura there is no principle difference between Shockley and Tamm states. Nevertheless, nowadays one categorizes a surface state being a Shockley or a Tamm state depending on whether or not the bandgap is inverted at the k point [27].

Surface states exist in the forbidden energy gap and are localized at the crystal's surface [27, 28]. In Tamm's original work that finding is based on terminating a Kronig–Penney potential. Nevertheless, the fact that surface states exist in the forbidden energy gap can be deduced from an even simpler model [27, p. 46], by

[5] If not two metals are adjoined.

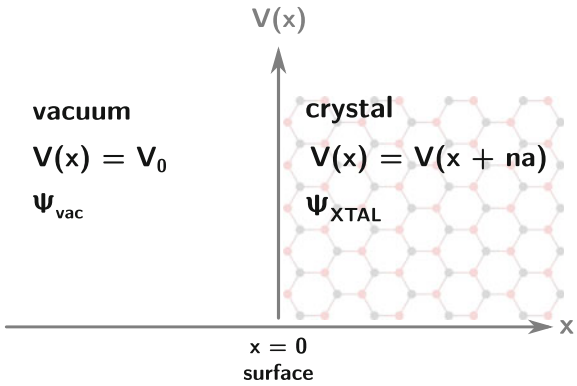


Fig. 2.4 Schematic diagram of an ideal crystal vacuum interface in one dimension. Inside the crystal (x > 0) the potential is periodic V(x) = V(x + na) according to the crystals translational symmetry. Outside (x < 0) V(x) = V_0 is simply constant. The wave functions inside (ψ_{XTAL}) and outside (ψ_{vac}) the crystal will be matched according to (2.27). Realistically the potential change from V_0 to V(x + na) will not be as abrupt and the first some unit cells will not necessarily have the crystal's periodicity

solely exploiting Bloch's theorem. Consider the example of Fig. 2.4, in which the wavefunctions in the respective regions are as follows.

$$\psi_{\text{vac}} = De^{k_0 x} \qquad k_0 = (V_0 - E)^{1/2} \tag{2.25}$$

$$\psi_{\text{XTAL}} = Au_{\text{k}}(x)e^{ikx} + Bu_{-\text{k}}(x)e^{-ikx} \tag{2.26}$$

here A, B and D are constants to be appropriately chosen to match the lattice Bloch waves u_{k}. To ensure a finite value of the norm of the wave function in the vacuum region for $x \to -\infty$ the solution must fall towards zero as in (2.25). Equation (2.26) is the general solution of the Schrödinger equation in the crystal, consisting of two Bloch waves. Now both wave functions and their derivatives have to be matched at x=0 leading to the following system of equations for the coefficients A, B and D:

$$Au_{\text{k}}(0) + Bu_{-\text{k}}(0) = D \tag{2.27}$$

$$A\left[u'_{\text{k}}(0) + iku_{\text{k}}(0)\right] + B\left[u'_{-\text{k}}(0) - iku_{-\text{k}}(0)\right] = Dk_0 \tag{2.28}$$

If (i) k in (2.26) is real, then the wave function ψ_{XTAL} is finite and the corresponding energy eigenvalue lies within one of the allowed energy bands. In this case, (2.27) and (2.28) are two equations for three parameters. Thus, one will always find a solution to match the wave functions of both regions. This makes every allowed solution for the energy of the infinite crystal also a solution for the semi infinite crystal. If on the other hand (ii) k in (2.26) is complex, then one of the summands in (2.26) and thus also ψ_{XTAL} will diverge for $x \to \infty$ unless the corresponding

coefficient A or B is also zero. In that case, (2.27) and (2.28) are two equations for two coefficient, which only has solutions for the electron energy E, if the equation system's determinant vanishes for that value. Therefore, these solutions correspond with energy values in the forbidden energy gap of the infinite crystal. Moreover, the solutions will exponentially fall off inside the crystal, though in an oscillatory manner caused by $u_k(x)$.

Having discussed that surface states exist in the bandgap, one thing must not be confused. The statement relates to the bandgap at a specific point of the reduced zone scheme. Upon sketching band diagrams often a whole band is projected onto a single axis. In such illustrations surface states may very well overlap with bands.

2.2.4.2 Electron Band Tails

As it was already pointed out, electronic band tails arise due to disorder of a crystal. Consequently, many of the contributions originate from the field of amorphous materials and melts. Among the most prominent to investigate the topic were Mott and Anderson for which they later became Nobel laureates in 1977.

For the present thesis of most interest is the density of states (DOS) of disordered solids. In order to derive expressions for $g(E)$ one usually employs the ansatz that the potential fluctuations due to disorder are Gaussian distributed.

$$P(V) = \frac{1}{\eta\pi} \exp\left(-\frac{V^2}{\eta^2}\right) \qquad \eta = \sqrt{2} V_{\text{rms}} \tag{2.29}$$

where V_{rms} is the root mean square of the distribution and thus a measure for the width of the potential fluctuations. Equation (2.29) is also sometimes called Gaussian white noise potential. E.g., Halperin and Lax discuss under which circumstances white noise Gaussian potentials are to be found [23, 29, 30]. Based on such a potential one can derive expressions for the DOS [21, 23–25, 31, 32]. It is found that the results for the DOS critically depend on two factors: First, how long ranging the impurity potentials are or more general the correlation length of the disorder L. Second, the functional form of the DOS in different energy regimes of the tail was found to be different [23]. In the limit that the de Broglie wavelength $\lambda = \hbar/(2m|E|)^{1/2}$ is long compared to the finite correlation length of the disorder, Cardy et al. [31] have shown that the DOS behaves as:

$$g(E) \sim |E|^{d(5-d)/4} \exp(-const \cdot |E|^{2-d/2}) \tag{2.30}$$

where d is the dimensionality of the system. In the opposite limit of $L >> \lambda$, John et al. [32] derived the following form for the DOS:

$$g(E) \sim |E|^{d} \exp(-|E|^2/2\, V_{\text{rms}}^2) \tag{2.31}$$

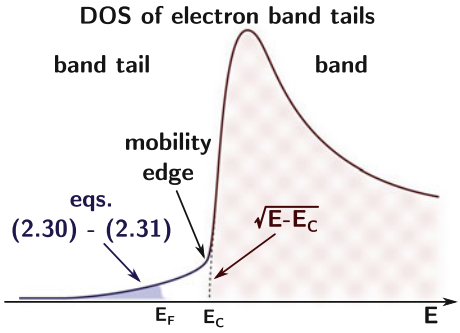


Fig. 2.5 Electron band tail of the conduction band due to disorder. The functional form of the DOS in the tail region is markedly different from the well known parabolic band approximation, $\sqrt{E - E_C}$, of the CB around E_C. Instead, the functional form is in between the two limiting cases of Eqs. (2.30) and (2.31). Furthermore, the states in band tails are localized, while the band states are delocalized. The mobility edge is the energy separating these regimes of differently conducting states

Within these two limits (cf. Fig. 2.5) and the different dimensionalities of the bulk crystal and the surface, regions falling off as $\exp(-E)$ may happen [33]. Indeed, this is the approximate experimentally found functional form of the GDOS/PES intensities investigated in Sect. 5.3.

Not central to this thesis, but for the interpretation and the implications of the present data, is that states in band tails are localized, while band states are delocalized over the whole crystal [34, 35]. Thus, transport through band tails depends on the distribution and percolation paths of imperfections in the crystal. Hereby, it is similar to the previously mentioned hopping transport models. For further discourses on electron band tail transport see [36–38].

2.3 Models and Processes of Energy–Level Alignment

In the previous sections the electronic structure of inorganic and organic semiconductors as individual materials was discussed. But for a concise understanding of the electrical properties of devices another prerequisite is to know the electronic structure and energy–level alignment at interfaces. Ultimately, the energy–level alignment at interfaces is a function of the charge rearrangement upon formation. However, the charge rearrangement can be extremely complicated. It depends on several aspects as bond formation, intrinsic dipoles, the position of the Fermi level, the electronic structures of the individual components plus the hybridization between them upon contact formation and lastly molecular distortions or strain due to lattice mismatch. Here, it should be also stressed that the charge distribution at interfaces is connected to the capacitance of the system [39]. Just as a single example: Interfaces with or without charge transfer behave differently concerning high frequency alternating currents.

In order to comprehend energy–level alignment and charge distribution at interfaces, here, certain processes and limiting cases will be presented individually. Accordingly, Sect. 2.3.1 will define the Fermi level followed by a thorough discourse of band bending in Sect. 2.3.2. Then, Sects. 2.3.3 and 2.3.4 will treat two different schemes of energy–level alignment, i.e., vacuum level alignment and Fermi–level pinning. Section 2.3.5 will explain the push back effect. Lastly, the importance of molecular film structure for energy–level alignment is elucidated in Sect. 2.3.6.

Almost exclusively, interfaces within this thesis are planar and homogenous. Therefore, potential changes occur in z only, which is normal to the interface. For the simplest case of only an interface dipole the situation resembles the one of a single plate capacitor. The energy–level shift can then be calculated via the Helmholtz equation as a function of the charge density σ at the individual sides of the interface dipole and of the spacing d:

$$\Delta\phi = \frac{e \cdot d \cdot \sigma}{\epsilon_0 \epsilon_\mathrm{r}} \qquad \Delta\phi = \frac{e \cdot n \cdot \mu_\perp}{\epsilon_0 \epsilon_\mathrm{r}} \tag{2.32}$$

ϵ, ϵ_0 and e are the relative and vacuum dielectric permittivity and elementary charge. The right hand side equation conceives the same situation to be cause by n dipoles of strength $\mu_\perp$ in direction of the interface normal. Equation (2.32) is a specialized version of Poisson's equation. For more complex potential curves across an interface, one can always slice the potential curve into infinetesimal small slabs in z, in which the potential changes linearly. This is equivalent to an appropriate concatenation/superposition of (infinetesimal small) plate capacitors. A prominent example, in which such an ansatz is necessary is band bending. Historically, such smeared out potentials were first observed for solid liquid interfaces and referred to as electrical double layers. Nevertheless, the terminology is also sometimes used in the field of semiconductor (metal) heterojunctions. It was already recognized in that context, that the charge distribution/density not only determines the energy–level alignment at interface, but also the capacitance [39]. Due to explaining the potential curve as a concatenation of plate capacitors such a connection is obvious.

2.3.1 Doping and Fermi–Level

The Fermi level (E_F) is a concept of statistical physics denoting the total chemical potential of electrons (μ) of a thermodynamic system [17, pp. 759 sqq]. In thermodynamic equilibrium all redistribution of particles and thus also electrons has come to an end. Then the electron chemical potential is equal throughout the system, otherwise electron redistribution would be resumed. Therefore, for a system in thermodynamic equilibrium there exist a single constant Fermi level. Care must be taken to differentiate the Fermi level from the Fermi energy, which simply is the energy of the highest occupied electron state at T=0, which is equivalent to $\mu(T = 0)$.

In particular the Fermi level determines the occupation probability of Fermionic states via the Fermi–Dirac distribution (also Fermi–Dirac statistics) [17, pp. 561 sqq]. This means that if the density of states (including dopants) is known, all of the internal charge distribution can be calculated provided the Fermi level is known. It is this, what makes the Fermi–Level the key parameter to the understanding of electrostatics inside a material and thus also of energy–level alignment.

This subsection aims to lay the definitional groundwork of semiconductor physics necessary to calculate the Fermi–Level. But also emphasis is put on understanding how the Fermi–Level is functionally entangled with the charge densities, which is fundamental for solving Poisson's equation in general or, more particular, to calculate band bending in crystals in Sect. 2.3.2:

Using Eq. (2.33) one calculates the number of electrons in the conduction band n and number of holes in the valence band:

$$n = \int_{E_C}^{E_{top}} g_C(E) f(E) dE \qquad p = \int_{E_{bottom}}^{E_V} g_V(E)[1 - f(E)] dE \tag{2.33}$$

$$n \simeq \frac{2N_C}{\sqrt{\pi}} F_{1/2}(\eta_C) \qquad p \simeq \frac{2N_V}{\sqrt{\pi}} F_{1/2}(\eta_V) \tag{2.34}$$

$$\approx N_C e^{(E_F - E_C)/k_B T} \qquad \approx N_V e^{(E_V - E_F)/k_B T} \tag{2.35}$$

where g_V and g_C are the DOSs of the valence and conduction band, E_C and E_V bottom and top energies of valence and conduction band respectively and $f(E)$ the occupation probability given by the Fermi–Dirac distribution. Line two results from using a parabolic band approximation, using electron and hole effective masses m_e^* and m_p^* and reformulating with the abbreviations/definitions (2.36)–(2.37) (displayed below) for the effective densities of states N_C and N_V and the Fermi–Dirac integral $F_{1/2}(\eta)$ (cf. [40], pp. 112sqq). Equation (2.35) in the last row is approximating Fermi–Dirac statistics by Maxwell–Boltzmann statistics, which is reasonable for nondegenerate semiconductors. Such are defined [40, p. 115] as that the Fermi level is farther than $3\,k_B T$ displaced into the bandgap.

$$N_C = 2\left(\frac{2\pi m_n^* kT}{h^2}\right)^{3/2} \qquad N_V = 2\left(\frac{2\pi m_p^* kT}{h^2}\right)^{3/2} \tag{2.36}$$

$$F_{1/2}(\eta) = \int_0^\infty \frac{\xi^{1/2} d\xi}{1 + e^{\xi - \eta}} \quad \eta_C = (E_F - E_C)/k_B T \quad \eta_V = (E_V - E_F)/k_B T \tag{2.37}$$

In the same fashion one calculates the number of ionized donors and acceptors N_D^+ and N_A^- via summing over all different doping species i and applying Fermi–Dirac statistics on their numbers N_{D_i} and N_{A_i}. Values of 2 and 4 for the degeneracy factors of donors and acceptors g_{D_i} and g_{A_i} are physically justified for most cases [40]:

$$N_{\mathrm{D}}^{+} = \sum_i \frac{N_{\mathrm{D_i}}}{1 + g_{\mathrm{D_i}} e^{(E_{\mathrm{F}} - E_{\mathrm{D}})/k_{\mathrm{B}}T}} \qquad N_{\mathrm{A}}^{-} = \sum_i \frac{N_{\mathrm{A_i}}}{1 + g_{\mathrm{A_i}} e^{(E_{\mathrm{A}} - E_{\mathrm{F}})/k_{\mathrm{B}}T}} \tag{2.38}$$

At every point the sum of these four charge densities, i.e., the total charge density, constitutes the sources and sinks of the electric field. By this (and possibly existing boundary values) the semiconductor's internal potential is defined via Poisson's equation (where Δ is the Laplace operator):

$$\left[n - p + N_{\mathrm{D}}^{+} - N_{\mathrm{A}}^{-}\right] = \frac{\rho}{\epsilon} = -\Delta\phi \tag{2.39}$$

This equation is also the basis for the discussion of band bending in Sect. 2.3.2. If band bending occurs Eq. (2.39) is not equal to zero everywhere, i.e., there are areas of net charge, where the crystal is not neutral. However, it is safe to assume, that areas infinitely deep inside the crystal (or sufficiently deep for real crystal) are neutral, otherwise charge neutrality of the macroscopic system would be unrealistically broken. In the neutral areas one can then simply set (2.39) zero and solve for the Fermi level, which is contained implicitly in all terms on the left hand side. This methodology now enables one to calculate the Fermi level via (Mathematica syntax):

$$E_{\mathrm{F}} = \mathrm{FindRoot}\left[\left(n - p + N_{\mathrm{D}}^{+} - N_{\mathrm{A}}^{-}\right) == 0,\, E_{\mathrm{F}}\right] \tag{2.40}$$

The Position of the Fermi level in ZnO ZnO is natively n doped [41–56]. This results from the fact that the most common crystal defects occurring during growth or common impurities act as n dopants [48, 54, 57]. The most prominent examples are of course oxygen vacancies and zinc interstitials resulting from oxygen deficient growth requirements as well as hydrogen, which is known to diffuse into the crystal and act as a shallow donor with a binding energy of 30 meV [43–47]. But also complexes with nitrogen (e.g., Zn_I–N_O) act as shallow donors [42, 53, 55]. To p–type dope ZnO has proven difficult [58–60]. In fact efforts so far have failed or only accomplished some compensation of the n dopants [61–65]. To this thesis however this adds some degree of reproducibility, since native doping with a density of $10^{17}\,\mathrm{cm}^{-3}$ to $10^{18}\,\mathrm{cm}^{-3}$ by shallow donors of 30 meV to 60 meV binding energy will always render the Fermi level and conduction band to be spaced about 100 meV.

2.3.2 Band Bending

Band bending arises from differences in charge concentrations. Wherever gradients of a charge carrier concentration occur, carriers will start to diffuse, smearing out the charge distribution, finally making it continuous and in the limit of infinite time also constant. The reason for this diffusion is that for non constant charge distributions there are less permutations to place the charges in the system than for constant distributions. This corresponds with fewer configurations/microstates of the partition

function and then also smaller entropy, which usually renders such charge distributions unfavored. However, while diffusion drives the system towards a new state such trend is counteracted by electric fields arising. Since for the present thesis the particles of interest are charges, i.e., they are not neutral, diffusion leads to electric fields and non neutral regions due to space charges. The resulting drift currents counteract the diffusion currents, which can be written as:

$$I_{\mathrm{n}}^{Drift} = q\mu_{\mathrm{n}} n E \qquad I_{\mathrm{n}}^{Diff} = q D_{\mathrm{n}} \frac{dn}{dz} \tag{2.41}$$

$$I_{\mathrm{p}}^{Drift} = q\mu_{\mathrm{p}} p E \qquad I_{\mathrm{p}}^{Diff} = q D_{\mathrm{p}} \frac{dp}{dz} \tag{2.42}$$

where q is a signed elementary charge, n and p electron and hole concentrations, μ_{n}, μ_{p} electron and hole mobilities and D_{n}, D_{p} electron and hole diffusion coefficients. For simplicity Eqs. (2.41) and (2.42) are restricted to the one dimensional case in z direction. The resulting electric field is of course linked with the charge densities via Poisson's equation (2.39).

The prime example of band bending is the case of a pn junction (cf. Fig. 2.6), in which the original concentration difference is due to the different doping concentrations and thus different n and p charge carrier concentrations on the individual sides of the heterojunction.[6] Leaving the charges as is, corresponding with neutral regions on both sides of the heterojunction, is only one possibility. Diffusion of some n and p carriers into the opposite regions increases the entropy and minimizes the system's energy. In effect both sides of the junction are not neutral anymore and the electric field due to the space charges balances the diffusion currents.

By Eqs. (2.41) and (2.42) n and p are in principle functions of spatial coordinates and time. However, here, one is only interested in the course of the band bending in thermodynamic equilibrium, i.e., the stationary solution. That particular solution is characterized by the diffusion current due to the concentration gradient exactly balancing the drift current by the resulting electric field [66, p. 46]:

$$I_{\mathrm{n/p}}^{Drift} = I_{\mathrm{n/p}}^{Diff} \tag{2.43}$$

There are in principle two ways to find the solution of thermodynamic equilibrium. Either one can integrate an initial condition over time to converge to the stationary solution. Or one exploits that in thermodynamic equilibrium the Fermi level is the same throughout the solid. The first approach is more complicated and relies on values for D_{n} and D_{p} with large uncertainty. Thus, the second route will be used, which mathematically resembles the standard boundary value problem of electrostatics. By nature the second route cannot gain information on the temporal evolution of the charge distribution into equilibrium, while the first method could. But as it was mentioned this information is not required here, anyway.

[6] The charges by ionized dopants N_{D}^{+} and N_{A}^{-} cannot diffuse.

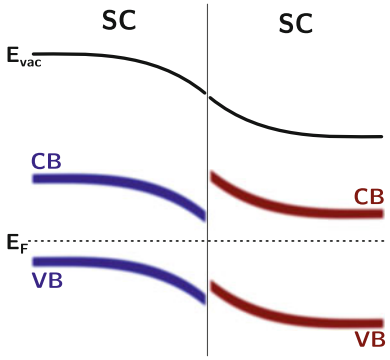


Fig. 2.6 Typical 1D band diagram including band bending in thermodynamic equilibrium. Depicted is the typical example of two adjoining semiconductors (SC), which are differently doped so that the Fermi level E_F is fixed (at infinity) at different positions relative to the bands. Due to the initial concentration difference (of n and p carriers) at the interface charges diffuse causing charge transfer and resultingly an electric field across the interface. In thermodynamic equilibrium the resulting drift current balances the diffusion current. The potential curve due to band bending (E_{vac}) will be continuous and differentiable, i.e., "bended". It is also apparent that in a band bending regime large potential shifts with effectively vacuum level alignment at the interface involving only marginal charge transfer could occur (see text)

Within this thesis planar interfaces of ZnO to organic molecules are investigated. Exploiting the x–, y–symmetry it is sufficient to calculate band bending in z direction only. The 1D solution in thermodynamic equilibrium typically leads to a band diagram as sketched in Fig. 2.6, in which the potential monotonously in– or decreases and saturates far away from the interface at both sides[7]. Nevertheless, one should keep in mind that, e.g., nanocolumns or surfaces exhibiting high roughness need to be discussed in the broader, three dimensional, nonuniform context.

2.3.2.1 ZnO Specific Considerations

Going into medias res with band bending in ZnO and HIOS systems some peculiarities are to be discussed. The paramount cause for band bending in this thesis is charge transfer across the HIOS interface and not differences in the doping level as for the case of the pn junction.[8] This is not so different as it might sound. In the pn junction the concentration differences cause band bending and thereby also charge transfer. At HIOS interfaces charge transfer occurring constitutes a concentration difference and subsequently band bending will partly rearrange the charge density

[7]Not necessarily differentiable at the interface, due to different dielectric permittivities at the individual sides of the junction..

[8]Note that band bending caused by different doping levels is definitely also present in ZnO originating from nonuniform doping towards the surface due to hydrogen diffusion [67]. Nevertheless, this effect is very small and hence it is neglected.

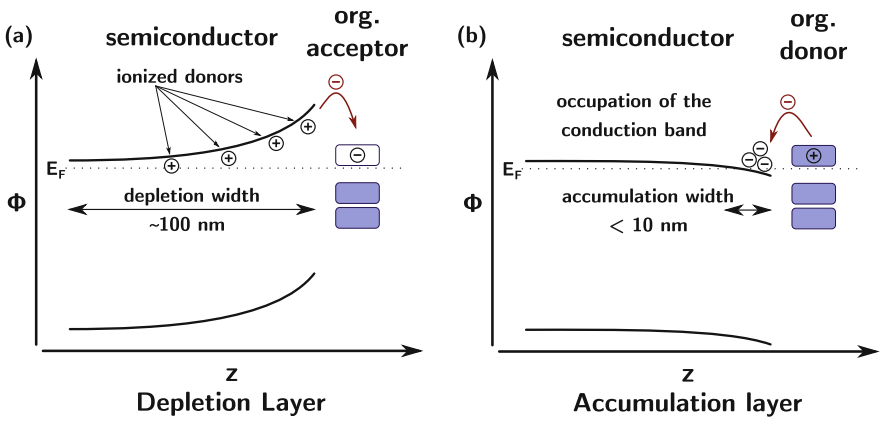


Fig. 2.7 Band bending at HIOS interfaces for **a** acceptor and **b** donor adsorption on ZnO. Band bending is caused by charge transfer across the interface. Electron transfer into molecular acceptors depletes the ZnO conduction band. Such charges originate from the native shallow donors leading to an extended (typically ca. 100 nm) space charge region, i.e., the depletion region. Electron transfer into ZnO by donors **b** occupies states of the conduction band. Due to the higher DOS of the CB accumulation widths are generally smaller

into equilibrium. Also surface adsorbates as hydrogen or hydroxy groups can be treated equivalently to organic adsorbates. The covalent bond to ZnO will never be fully symmetric so there must be a (small) net charge transfer causing band bending. This is exactly how the electrostatic instability of polar ZnO faces (cf. Tasker's rules and Sect. 5.1) can be resolved by surface adsorbates.

Band bending due to charge transfer across HIOS interfaces is sketched in Fig. 2.7 for acceptors and donors on ZnO. Electron transfer into molecular acceptors Fig. 2.7a depletes the ZnO conduction band. The transferred charges from the conduction band originate from the native shallow donors of ZnO. Therefore, not arbitrarily many charges can be extracted from a given volume close to the interface. Instead, the more charges transferred the deeper the depletion region will penetrate inside the ZnO crystal. How deep is solely governed by the density of donors and the total charge transfer. For typical scenarios of this work, i.e., native doping concentration and some 0.1 eV upward band bending, the depletion region will be of the order of 100 nm.

The situation is completely different for molecular donor adsorption on ZnO depicted in Fig. 2.7b. Electrons donated into ZnO occupy states of the conduction band having a much larger DOS than the dopants. This effectively confines the extra charges in close proximity to the interface as opposed to the case of molecular acceptor adsorption. Therefore, reasonable accumulation layer widths are much below 10 nm. Correspondingly, the net dipole per transferred charge is also much smaller than for acceptor adsorption and downward band bending shifts very limited. This limitation of downward band bending is much potentiated by the n type nature of ZnO: Since E_F is only ~ 100 meV spaced from the CBM the bands cannot be significantly

downward bended before E_F crosses the conduction band edge. This leads to further heavy occupation of the CB hindering downward band bending.

If depicting or inspecting only the ZnO part of adsorption induced internal band bending, charge distributions as the one in Fig. 2.7 might be a little unintuitive at first sight, for instance, that electron accumulation at the ZnO surface causes downward band bending shifts. However, one must not forget the countercharges on the molecules. In that sense, instead of understanding those accumulated electrons to pose a barrier to overcome so that the potential should go up, it is correct to think that those electrons more and more compensate the field of the countercharges on the molecules, which is why the band bending points downwards.

2.3.2.2 Intra–Organic Band Bending

Of course the charge transfer across a HIOS interface will in principle also cause band bending in the adsorbed molecular film. While intra organic band bending is also governed by the interplay of drift and diffusion currents, those behave different for organic than for inorganic semiconductors: Charge carriers in organic semiconductors are typically strongly bound by some 100 meV, due to the relaxation of the organic semiconductors charge distribution in response to the extra charge. In consequence conduction in organic semiconductors usually exhibits inferior mobilities and hopping transport as compared with higher mobilities and band transport in inorganic semiconductors [5]. Therefore, the balance of drift and diffusion currents (2.41)–(2.42) will be expectedly very different and hence also the form of the band bending.

Indeed, among the many studies of organic semiconductor interfaces a lot find no band bending with the charge density confined to the first organic layer only [68–72]. Other studies though do find energy–level shifts occuring between subsequent layers beyond the monolayer, which is attributable to intra organic band bending [72–78]. It should be mentioned though that if measurements are done by PES there exist some ambiguity: For film thicknesses of only a few nm such energy differences can be assigned to either band bending or differences in photohole screening. Recently, the transition between those two extremes of intra organic band bending being present or not has been reviewed by Oehzelt et al. [79]. Band bending being present or not is found to be two limiting cases dependent on the molecular DOS. Except for the discretization to account for the distinct molecular layers, the methodology used is very similar to the one presented in the upcoming Sect. 2.3.2.4, i.e., in thermodynamic equilibrium. This proofs, that intra-organic band bending is not different from inorganic band bending, but the underlying processes should be rather understood to happen on a mesh instead of in a continuum. Nevertheless, one should note that these are just simple models. Only two issues not included shall be mentioned: Due to the strong relaxation energies of organic semiconductors out of equlibrium conditions are more probable. Also placing charges in a molecular layer might significantly (locally) change its DOS.

2.3.2.3 The Depletion Approximation

Correct band bending potential curves as well as the corresponding charge distribution and electric fields are complex functions of the sample geometry, the doping concentrations and the DOS in general. Therefore, usually simple algebraic equations are unsuited to solve the problem. Yet for depletion regions one can in some cases derive such a form within the depletion approximation [66, p. 49]. First, it requires that the problem is treatable in 1D, meaning that the sample is homogenous in x and y. Furthermore, the depletion approximation usually considers the doping concentration constant throughout the crystal.[9] Concerning the charge carrier densities in the depletion region the approximation uses the following assumptions (here quoted for the case of ZnO, in which electrons are the majority charge carriers): Within the depletion region the majority charge carriers have been removed ($n(z) = 0$) and all donors are ionized ($N_\mathrm{D}^+ = N_\mathrm{D}$). Outside of the depletion region charge neutrality is given. Importantly, this implies that the depletion region (and the charge densities, electric fields and potentials) takes an abrupt end. The success of this approximation stems from the fact that upon upward band bending not only the energy levels of the bands, but also the dopant energy levels are bended upwards. Since occupation is governed by the Fermi Dirac distribution and E_F unchanged indeed both the dopant levels and the conduction band are ideally zero occupied. In consequence the total charge density in the depletion region is $N_\mathrm{D}^+ = N_\mathrm{D}$. Vice versa the same rationale holds for hole majority charge carriers and ionized acceptors $N_\mathrm{A}^- = N_\mathrm{A}$.

Accordingly, the total charge density in depletion approximation is a step function as sketched by the black curve in Fig. 2.8a. The end of the depletion region is sharp and indicated by w. For comparison the grey curve indicates the unapproximated course of the total charge density. Evidently, in close proximity to the interface the depletion approximation yields the correct charge density. But inside the crystal, at the nominal end w of the depletion region, deviations occur. It is there, where the transition from net charged volumes to neutral volumes occurs and using correct Fermi Dirac statistic matters.

The simple form of the charge density $\rho(z)$ allows to derive an algebraic equation for the potential shift $\Delta\phi$ in dependence of the charge transfer δq. Once integrating the constant charge density ρ to the end of the depletion region w yields a linear trend for the electric field as depicted in Fig. 2.8b. Twice integrating results in a quadratic behavior of the potential shift $\Delta\phi$:

$$\Delta\phi = \frac{eN_\mathrm{D}w^2}{2\epsilon} \qquad w = \frac{\delta q}{N_\mathrm{D}} \tag{2.44}$$

where $\epsilon = \epsilon_0 \cdot \epsilon_\mathrm{r}$ and N_D is the doping concentration. For geometric reasons w can trivially be calculated as in (2.44) from δq and N_D alone. Concerning the units

[9] Note that it is commonly omitted to name this criterion. Nevertheless, most integrations shown are based on constant N_D and N_A. Otherwise one will not arrive at (2.44), but has to find the antiderivative functions of N_D and N_A, which could still prove much easier than solving the unapproximated problem.

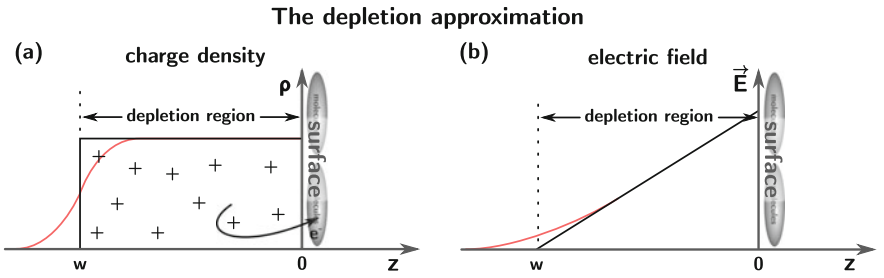


Fig. 2.8 When band bending occurs actual charge densities and thus electric fields and potentials (*grey lines*) might be so complicated that an analytical solution is impossible. **a** In depletion approximation (*black lines*) one assumes, that up to a certain depth w from the junction/surface all dopants (constant concentration) are fully ionized and their charges extracted from that region, i.e., the region has a constant net electric charge ρ. Beyond w the net charge abruptly falls to zero leading to **b** no electric field outside the depletion region. Within the region however the electric field increases linearly due to the constant charge density ρ. Finally this leads to a quadratic law for the electric potential

one should mind that reasonable charge transfers δq are in units of charge per area. Substituting w into the equation for $\Delta\phi$ leads to a formula quadratic in δq and inverse proportional in N_D. Therefore, band bending is expected to be influenceable by changing the doping concentration. This hypothesis will be tested in Sect. 5.2.1.1 and further consequences discussed.

The depletion approximation is highly successful in explaining molecular acceptor adsorption on ZnO. In particular the extend of the depletion region can be easily estimated, which is important for understanding ZnO (surface) conductivity. Deviations from the real charge distribution occur buried at depth w. Note that such buried deviations will still also influence the potential at the surface. In which way the real potential at the surface deviates from the one estimated within the depletion approximation can be deduced by the following rationale: The depletion approximation assumes an abrupt step in the charge density while the real distribution will always be a little more extended. Hereby, the effective dipole of those outermost last charges transferred will in reality be a little larger too. Therefore, the depletion approximation will always minimally underestimate $\Delta\phi$ for a given charge transfer δq. Similarly, one can also qualitatively understand that (upward ZnO) band bending produces much larger $\Delta\phi$ shifts per charge transferred as compared with confined interface dipoles. Consequently, in anticipation of the upcoming discussion of different energy–level alignments schemes Fig. 2.6 illustrates, that by band bending large $\Delta\phi$ shifts with marginal charge transfer and virtually vacuum level alignment at the interface are possible.

2.3.2.4 Numerical Solution of HIOS Band Bending: A Continuum Model in Thermodynamic Equilibrium and 1D

In many cases it is not possible to find an analytical solution for the course of the band bending. The depletion approximation is also not suited for all situations. Therefore, sometimes, the only practical way is to find a numerical solution. "Solution" in the following will relate to the potential ϕ, since it governs the other quantities of interest $\vec{E}$ and ρ.

As it was mentioned before, for this thesis one is interested in the solution in thermodynamic equilibrium, in which the Fermi level is defined and constant throughout the material. Also by using the introduced methodology one calculates band bending in a continuum model assuming it has no atomistic, discrete or even quantum mechanical character.[10] Furthermore, all HIOS interfaces of this work were planar, meaning that, due to symmetry, it suffices to base the upcoming discourse on Poisson's equation in one dimension:

$$-\frac{\partial^2\phi}{\partial z^2} = \frac{\partial E(z)}{\partial z} = \frac{\rho}{\epsilon} = \frac{e}{\epsilon}\left[n(z) - p(z) + N_{\mathrm{D}}^{+}(z) - N_{\mathrm{A}}^{-}(z)\right] \tag{2.45}$$

What is still missing for a unique solution are the boundary values. There are multiple possibilities how one can formulate those. The two most relevant ones for this work are specifying either a certain amount of charge transfer or the band bending shift at the surface, since this is experimentally assessable. Of course, both require that the potential and electric field vanishes in the bulk of the crystal, i.e., at infinity. The former case, is a Neumann type boundary condition, since by a certain charge transfer across the interface the electric field at the surface is also defined. The latter case, of specifying the total band bending shift at the surface is a Dirichlet type boundary condition.

For this thesis, problems of such kind will be numerically solved using Mathematica. The corresponding program code is listed in Appendix E. The charge densities within Poisson's equation (2.45) were implemented by using Fermi Dirac statistics. In particular, the densities of ionized dopants are calculated via (2.38) using degeneracies of 2 and 4. Charge densities of the valence and conduction band are calculated within a parabolic band approximation using (2.34). Several parameters, as dopant densities, their binding energies or the dielectric constant can freely be chosen to fit the appropriate material, but are constant throughout solving the differential equations (cf. lines 9–42).

The major difficulty is that Mathematica cannot directly solve the present boundary value problems. Most problematic is that the boundary conditions at infinity $\phi(\infty) = 0$ and $\phi'(\infty) = 0$ do not help to constitute a defined starting point. From those NDSolve cannot simply numerically integrate, which would be an initial value

[10] Particularly this latter point might be problematic as the results will show: Given a downward band bended situation in ZnO, charges are confined within 1–2 nm from the surface (see Fig. 5.30). Potentially, this 2D electron gas [80] has completely new quantum states, which changes the behavior of the internal ZnO band bending.

problem. Therefore, in practice the problem has to be reformulated to some sort of FindRoot operation, finding both $\phi(0)$ and $\phi'(0)$,[11] encapsulating the following differential equation (Mathematica syntax; case $\phi(0)$ unknown):

$$\text{NDSolve}\left[\left(n - p + N_{\text{D}}^{+} - N_{\text{A}}^{-}\right) == -\phi''(z),\ \phi'(0) == |\vec{E}(0)|,\ \phi(0) == xx\ eV\right] \tag{2.46}$$

While with this the general route of the code listed in Appendix E is outlined, there are several practical pitfalls to mind: The termination condition for the enclosing FindRoot operation is that at a value z_{end} inside the crystal both $\phi(z_{\text{end}}) = 0$ and $\phi'(z_{\text{end}}) = 0$ must be zero. For a given $\phi(0)$ using on the one hand a too steep value for $\phi'(0)$ yields ϕ crossing zero, but not converging to it. On the other hand using a too flat value for $\phi'(0)$ the potential ϕ yields an extremum, but offsetted from zero. In the first case $\phi(z_{\text{end}}) = 0$ is fulfilled, but not $\phi'(z_{\text{end}}) = 0$. In the latter case $\phi'(z_{\text{end}})$ is zero, but not $\phi(z_{\text{end}})$. Therefore, one cannot use a single termination criterion of either $\phi(z_{\text{end}})$ or $\phi'(z_{\text{end}}) = 0$ for both sides of the FindRoot operation approaching the physically correct value. Unfortunately, it is not possible to specify more than one termination criterion for Mathematica's NDSolve. Also NDSolve does not allow to employ a boolean differentiation between the different cases. Moreover, a termination criterion of $|\phi(z_{\text{end}})| + |\phi'(z_{\text{end}})| = 0$ is mathematically correct but numerically unstable. To circumvent such problems the actual implementation of the FindRoot operation encapsulating the NDSolve uses a symmetric divide and conquer algorithm to bisect the correct missing boundary value (lines 89–99). This approach allows to "outsource" the mentioned boolean differentiation from the NDSolve call. Lastly the code lines 47–50 realize a rainbow table for the Fermi–Dirac Integral $F_{1/2}$ (2.37) to speed up solving the nested FindRoot[NDSolve[...]] operation.

2.3.3 *Vacuum Level Alignment*

Vacuum level alignment (or also the Schottkey–Mott limit) describes the limiting case of energy–level alignment, where there is no jump in the potential at the interface [81]. This picture is well suited to describe non– or very weakly interacting interfaces. This can be understood in the following logic: The position of energy levels of two individual systems, be it organic or inorganic semiconductors, can be defined with respect to the vacuum level E_{vac}. Bringing the two systems into contact, the question is how the energy levels at the interface align. In the limit of no interaction[12] no charge is redistributed and thus the potential unchanged across the interface. Consequently, the energy levels at the individual sides of the interface can both be calculated with respect to the now common constant potential, i.e., the vacuum level.

[11] One is known, the other will be solved for.

[12] Of course a little interaction must always be present, otherwise the two system would not stick together.

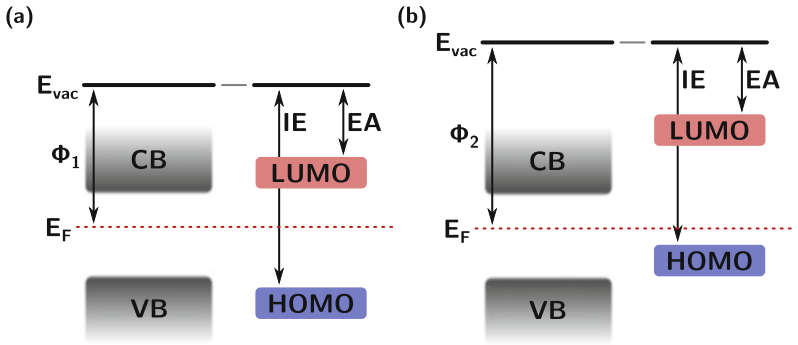


Fig. 2.9 Energy–level diagrams within the model of vacuum level alignment for HIOS structures. **a** An organic semiconductor aligns its vacuum level with the vacuum level of the underlying inorganic substrate, which is defined by the work function ϕ_1. The energy level position of the organic semiconductor's HOMO and LUMO can then simply be calculated knowing the ionization energy and electron affinity respectively. Increasing the substrate's initial work function to ϕ_2 as in **b** will lift the energy levels of the organic semiconductor

Such a vacuum level alignment situation is depicted in Fig. 2.9 for a HIOS system comprising an organic semiconductor on an inorganic one. By the work function ϕ the position of the vacuum level can itself be described with respect to the Fermi level. This is advantageous, since the Fermi level is a constant throughout both systems in contact[13] (see Sect. 2.3.2). Therefore, in (a) the position of E_{vac} is defined by ϕ_1. The organic semiconductor on top vacuum level aligns so that the energies of HOMO and LUMO w.r.t. E_F can be calculated via:

$$E_{\text{HOMO}} = \phi - IE \qquad E_{\text{LUMO}} = \phi - EA \tag{2.47}$$

where IE and EA are the ionization energy and electron affinity of the organic material. The advantage of the Schottky–Mott limit is, that the interfacial energy–level alignment can be determined/predicted from properties of the individual systems. Changing the work function of the substrate, e.g., by employing another material or substrate modification, the situation changes as shown in Fig. 2.9b. Then, due to the higher ϕ_2, HOMO and LUMO come to lye at higher energies according to Eq. (2.47). The characteristic behavior of linearly scaling the energy levels of an organic semiconductor by changing the work function of the substrate underneath, is abstracted in the slope parameter S [82, 83]. For vacuum level alignment S is supposed to be one, but S is also used in other contexts, where it differs from one.

It is quite obvious that the Schottky–Mott limit can only be fulfilled in a limited range of substrate ϕ. If the substrate ϕ is too high (low), the HOMO (LUMO) would be above (below) E_F. Since the occupation of the HOMO (LUMO) is governed by the position of the Fermi level such situation would lead to charge rearrangements

[13] In thermodynamic equilibrium.

and thus interface dipoles. Such pinning at the frontier molecular energy levels is called Fermi–level pinning and will be discussed in Sect. 2.3.4. But even with ϕ in the allowed range between the critical ϕs for HOMO or LUMO pinning, one can still encounter Fermi–level pinning at gap state density of states. Another effect why one often does not find Eq. (2.47) fulfilled is the push back effect, occuring most prominently for organic materials deposited onto metals (see Sect. 2.3.5). For push back, though, one could argue that it is only the surface dipole that is reduced. The actual potential across the interface might actually not change, which would be in accordance with the above given definition of vacuum level alignment. This illustrates some ambiguity in usage of the term vacuum level alignment. Strictly, the alignment occurs at the common punctual potential of the interface (plane). The problem is that this relevant potential can not always be described by the vacuum level prior to adsorption. This is due to induced changes of the surface potential upon contact formation, e.g., by push back or band bending. The ambiguity arises from using the term vacuum level or the closely related surface potential without proper definition [73, 84]. Even more problematic, neither of those terms is intuitively definable at an interface, since there is no surface and also no vacuum anymore. As already mentioned only sometimes their definition at the individual seperated systems coincides with what would be better named "interface potential".

Due to the discussed reasons, vacuum level alignment is most often observed for organic organic heterojunctions [71, 85–87]. Furthermore, organic materials on substrates with negligible push back, e.g., weakly doped semiconductors or contaminated, passivated surfaces, are predestined for vacuum level alignment [88].

2.3.4 Fermi–Level Pinning

As it was already pointed out in the previous section, the vacuum level alignment scheme does not always hold. Among the many reasons for this behavior, probably the most important one is Fermi–level pinning. Generally, Fermi–level pinning refers to the effect that the energy level positions become fixed if the Fermi level intersects with (sufficiently large) DOS at the interface.

To understand Fermi–level pinning, it is instructive to consider the process of closing in the two sides of an interface into contact. It does not make a difference whether the materials on each side are either inorganic or organic materials. With both sides still apart, but not in the far field of the opposite surface (cf. Fig. 3.3), the vacuum levels of the two materials are aligned. Upon moving closer into intimate contact (but still considering the systems apart) push back may occur. Alignment at the interface then occurs not at the vacuum levels before contact, but at the current surface potentials. At that stage it can accur that occupied states of one side of the interface come to lye above E_F or, vice versa, the unoccupied states of one constituent to be below E_F. Then, however, the formerly occupied (unoccupied) states would be emptied (filled). This process is governed by Fermi–Dirac statistics and the relative position of the energy levels to the Fermi level. Emptying or filling states within

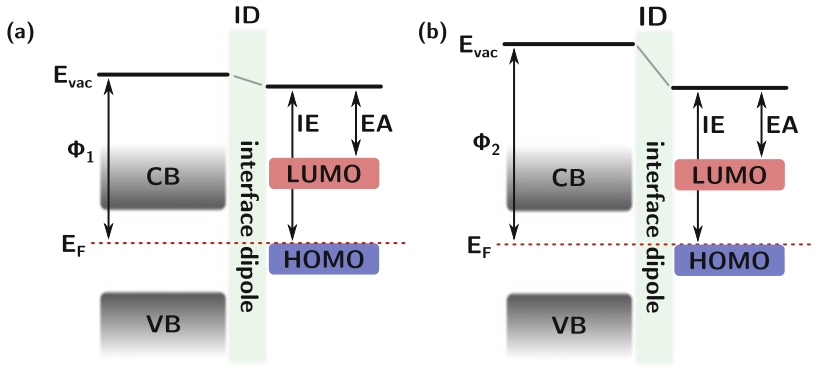


Fig. 2.10 Sketch of Fermi–level pinning for a HIOS system, i.e., an inorganic material to the left and an organic one to the right. **a** Fermi–level pinning occurs if the substrate's work function ϕ_1 is larger (lower) than the ionization energy (electron affinity) of the organic. Then, the materials cannot vacuum align, since the HOMO (LUMO) of the organic would be situated above (below) the Fermi level E_F. In that case, holes (electrons) are transferred into the HOMO (LUMO) causing an interface dipole. This realigns the organic's HOMO (LUMO) below (above) the Fermi level, reestablishing thermodynamic equilibrium. **b** Using a higher initial work function ϕ_2 simply causes a larger interface dipole, but aligns the organic's energy levels at virtually the same energy as in **a**

formerly neutral regions causes charge transfer across the interface. Correspondingly, interface dipoles and/or band bending occurs. This process continues until, eventually, the energy levels are in positions, where their occupation is in equilibrium. The occupation/deoccupation of those energy levels effectively fixes their positions close to, at or minimally overlapping with E_F. This is called Fermi–level pinning. The energy at which pinning occurs is called the pinning level.

Two different Fermi level pinned HIOS energy–level alignments are shown in Fig. 2.10. In (a) the inorganic semiconductor to the left exhibits a work function ϕ_1. If the organic semiconductor were to vacuum align with the inorganic semiconductor, its HOMO would be above E_F. A moderate interface dipole (ID) readjusts the energy levels downwards into equilibrium. In (b) the same organic semiconductor is put on a higher work function ϕ_2 inorganic substrate. Here, a larger interface dipole is required to bring the energy levels into thermodynamic equilibrium below E_F. The presented alignment is based on the assumption that the DOS associated with the molecular HOMO is (sufficiently) large. In that case, the position of E_F relative to the HOMO is effectively constant irrespective of the size of the interface dipole. Yet, for a small (enough) DOS the pinning level can significantly vary with the size of the required interface dipole, which is explained in the following text.

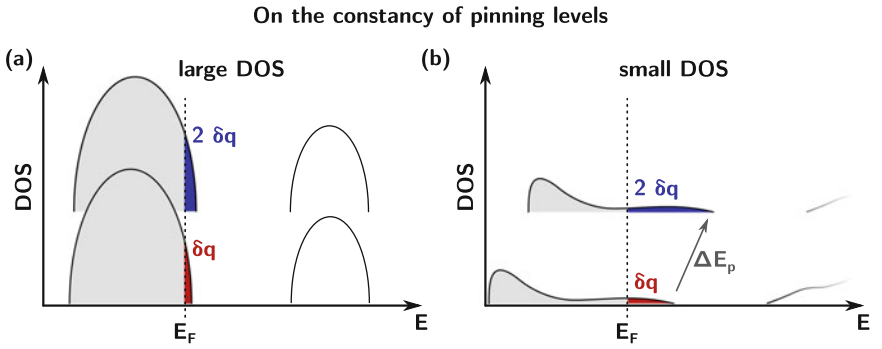


Fig. 2.11 Comparison of pinning levels for two different amounts of charge transfer for the cases of **a** large or **b** small DOS. Different amounts of charge transfer occur if different potential shifts are required to equilibrate the interface. In **a** a charge transfer δq depletes the large DOS within the region indicated in red. Twice the amount of charge transfer requires a larger energy region (*blue*) to be depleted. Yet, both regions are small, so that the positions of the energy levels are effectively independent of the required potential shift across the interface. This is different in **b**. Here the DOS is small, so that a larger charge transfer leads to a nonneglegibly larger depleted energy region. Consequently, the DOS is further upward shifted and pinning levels observed are different by ΔE_p

2.3.4.1 Fermi–level Pinning and Gap States

Another origin for Fermi–level pinning are gap states. This connection was already pointed out in 1947 by Bardeen [89] to explain the observed Schottky barrier heights. Pinning at gap states is of paramount importance for interfacial energy–level alignment for two reasons: First gap states are omnipresent, particularly at surfaces and interfaces. Second, since they are located in the gap, they are usually close to E_F and thereby influence or dominate the energy–level alignment.

Principally Fermi–level pinning at gap states is not different to the previously given rationales, since also gap states are DOS. However, typical peculiarities should be pointed out. First, Fermi–level pinning at band states will always cause band bending. For pinning at gap states, this is not necessarily the case. This depends on the localization of the gap states, whether they are confined to the interface or also exist in the bulk, but also on how deep the states are trapped in the gap (see Sect. 2.2.4). Second, it could be wrong to assume that the DOS is large. This is particularly true for the ultra low density of ZnO gap states, that are the topic of Sect. 5.3. Remember that for a large DOS the pinning level is effectively not dependent on the amount of charge transfer necessary for the potential shift to equilibrate the interface. For a small DOS, the energy region to be depleted (or filled) to supply the required amount of charge transfer could actually be not close to zero. Then different required amount of charge transfers, e.g., due to different substrate work functions, would lead to measurable different pinning levels E_p (see Fig. 2.11b). In that situation the term pinning might be misleading, since it implies an abrupt stop. Therefore, in such a context, arguments will be reformulated to "hindering" of energy–level shifts.

2.3.4.2 Pinning Levels of Organic Semiconductors

Pinning levels of organic semiconductors are commonly observed some few 100 meV away from the HOMO (LUMO) onsets, offsetted into the bandgap. Different mechanisms have been proposed for such behavior. In the integer charge transfer (ICT) model the pinning levels are, identified with the polaronic states of the organic semiconductor, which are offsetted into the bandgap [72, 90, 91]. However, recently a refined model of organic polaron levels was proposed [92]. An alternative explanation for the offsetted pinning levels is tailing of the organic semiconductors HOMO and LUMO levels [93]. In that picture the organic semiconductor is conceived as an imperfect solid. The tailing of the HOMO and LUMO is related to the disorder in the solid (see also Sect. 2.2.4). The tails can be of such low intensity that standard PES does not detect it, but still constitute enough DOS to determine the pinning level. For this model it should be recapitulated that for small DOSs the Fermi level might not be pinned but rather strongly hindered to move freely in the DOS tail.

2.3.5 Push Back

Many electronic alignment processes are influenced by the value of the work function. However, the work function of a material is not simply a constant, but depends itself on several properties of the material and surface (or interface). Of course, the value of the work function is also influenced by internal electric fields, as, e.g., band bending. For this subsection the contribution of the surface dipole (SD) to the work function will be the central point.

Quantum mechanically, there exist a non–vanishing, but exponentially decaying, probability for electrons to reside in the vacuum outside of the material. Thus, for reasons of charge neutrality, there will always be a net negative charge density above the surface and a net positive one in the material, due to the missing, spilled out electrons. The spill out of charge density can extend over several Å. That situation is depicted in Fig. 2.12a. Of course, such a charge density induces an electric field and potential change across the surface. The difference of the potential in the bulk of the material and far above the surface is called the surface dipole. Due to the nature of the charge distribution, surface dipoles always increase the work function. Differently sophisticated models can be devised to describe the explained situation. The most common discussion of the surface dipole is based on the jellium model [94, 95], which neglects the pointlike nature of the atomic nuclei and assumes a uniform background of positive charges. But also more advanced treatments including the lattice character and pseudopotentials have been developed [94], yielding good quantitative agreement with experiment. Ultimately, the problem of the surface potential is solved if the electron distribution is known. Hence, modern electronic structure calculations can also assess the effect.

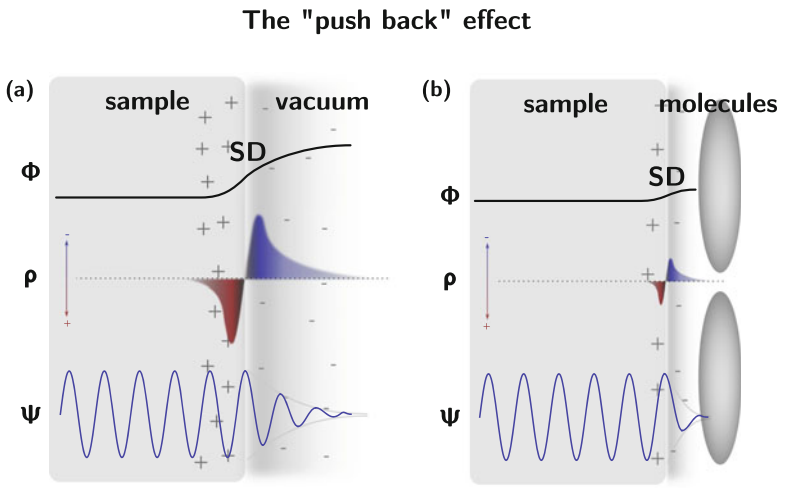


Fig. 2.12 Illustration of the push back effect. Electron wavefunctions do not abruptly fall off to zero at surfaces. Hence, electrons are also localized above the surface, outside of the sample. Such spilled out electrons leave the sample net positively charged yielding an electric field across the surface. The concomitant potential shift is termed the surface dipole (SD). Deposition of organic molecules onto surfaces leads to a reduction of the surface dipole. The reason is that spilled out electron density is pushed back, due to the pauli exclusion principle. This diminishes the surface dipole and the work function

Deposition of organic molecules onto clean metal surfaces often yields a reduction of the work function. That is even the case for deposition of only weakly interacting materials [96]. E.g., depositing rare gases on metals one still observes a significant lowering of the work function [97], despite the interaction being close to physisorption. These reductions of the work function are attributed to a lowering of the surface dipole due to the adsorbate layers. The molecules adsorbed change the potential above the surface, but most importantly, since electrons are Fermions, lead to Pauli repulsion of the spilled out electrons. Hence, the net charge density spilled out of the substrate is reduced and effectively also the surface dipole as it is shown in Fig. 2.12b. This behavior is referred to as push back or the pillow effect. Observed work function reductions attributed to the push back effect can be as large as ~1 eV [98–100] (pentacene on gold surfaces). For organic molecules on oxides one commonly observes a reduction by ca. 0.3 eV, which has also been attributed to pushback [101, 102]. The smaller size of the effect can be explained by the reduced charge density in the oxide's conduction band as compared with metals. It should be stressed again that the work function reduction by the push back effect is not an interface dipole. Interface dipoles may yet occur additionally. The push back effect alone, only reduces the surface dipole, which does not imply a potential change across the interface.

2.3.6 Molecular Film Structure

Several aspects of the structure of an organic thin film influence its electronic structure and interfacial energy–level alignment. Among those aspects are the molecular packing density and disorder, the electronic overlap between different molecules, the distribution of defect/dopant sites, the molecular orientation and inhomogeneity. Many of the mentioned properties are critically linked with the growth behavior of the organic film. Furthermore, the peculiar growth mode may influence what is seen by a measurement technique. Therefore, Sect. 2.3.6.1 will focus on organic thin film growth and Sect. 2.3.6.2 seperately discuss the influence of molecular orientation on energy–level alignment.

2.3.6.1 Growth Modes/Morphological Aspects

Within this work organic thin films are grown by molecular beam deposition from resistively heated quartz crucibles. Growth occurs under UHV conditions onto cleaned ZnO substrates or on such way precovered surfaces. During growth a constant flux of molecules is impinging onto the substrate. Behavior of molecules after hitting the surface depends on several substrate and organic material properties: Some of the molecules are reflected from the surface with the ratio expressed as the sticking coefficient. Others might simply stay in place covering the substrate or top precovered areas. Possibly, molecules have a tendency to coalesce, or vice versa. Diffusion of organic material on the surface could lead to closure of previous layers, but also preferential filling of defects/voids or final adsorption at special sites as step edges. Several studies exist to address the specific processes or growth in general [103–111].

The particular morphology and structure of deposited organic films formed is a balance between the molecule–substrate and molecule–molecules interactions. Furthermore, in non–equlibrium, the growth is a kinetic process depending on the energy of the impinging particles and the substrate temperature to mediate diffusion processes. In general one categorizes growth into three predominant growth modes, which are shown in Fig. 2.13:

(i) Frank–van der Merve growth: For this case substrate–molecule interactions outweigh the molecule–molecule interactions. Then molecules will grow in a layer–by–layer fashion, closing preceeding layers first. (ii) For the opposite case of superior molecule–molecule interactions the molecules nucleate to islands, which is called Volmer–Weber growth. (iii) There further exist an intermediate case (Stranski–Krastanov growth), in which one or a few closed monolayers are formed before subsequently island growth prevails. Here, the first closed monolayer(s) modifies the substrate–molecule interactions to a point that continued layer–by–layer growth is unfavorable.

Knowledge of the growth mode is critical for the interpretation of PES and NEXAFS data. Vice versa, certain conclusions about the growth mode can be

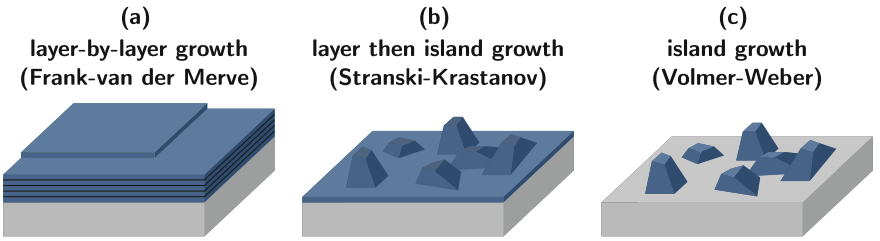


Fig. 2.13 Categorization of the global growth behavior into three main modes: **a** layer by layer growth, which is also called Frank–van der Merve: Each layer is grown successively. **b** Due to the interaction of the deposited material with the substrate the deposited material completely covers the substrate, but in a thicker regime clusters are formed. This is called Stranski–Krastanov growth. **c** the deposited material forms clusters on the substrate without fully covering the whole substrate area. New material is adjoined at/on the clusters instead of filling the empty patches on the substrate. Then one speaks of Volmer–Weber growth

obtained from these data. E.g., if deposited films exhibit Volmer–Weber growth observation of interfacial properties by PES or NEXAFS might be impossible, since both techniques are highly surface sensitive. Also for the strength of the substrate signal the growth mode has to be taken into account.

2.3.6.2 Molecular Orientation

As it was pointed out the molecular orientation of organic semiconductor films is also of relevance for interfacial energy–level alignment. This is mainly due to the surface potential of such films being dependent on the molecular orientation, which can be understood in a simple rationale: Considering on the one hand a face–on lying film the electron rich π–system of the organic semiconductor is faced towards the surface. On the other hand a standing organic semiconductor typically exposes hydrogen atoms towards the surface. In the latter case the surface potential barrier is reduced as compared to the barrier if the surface electron density is made up of the electron rich π–systems. Consequently, the differently oriented molecular films have different ionization energies. Or, to put it more generally, the molecular energy levels are at different positions with respect to the surface potential. Logically, for molecules as F4TCNQ or HATCN comprising highly electronegative outer cyano groups, standing orientation yields higher ionization energies than face–on orientation. Principally the effect is analogue to different crystal faces having different work functions [84, 112].

If now an organic layer were to vacuum align with the substrate then different orientations of the molecular film translate into different binding energies of its energy levels. That way for DH6T and 6T on Ag(111) it was found that the molecular energy levels are shifted relative to each other depending on whether the organic

film adopts a standing or lying orientation [113].[14] In contrast, if Fermi–level pinning prevails different molecular orientations of a layer can give rise to different final work functions/work function changes, but molecular energy levels at the same binding energy.

Note that formation of the different IEs is a collective effect of many adjacent molecules. Even formation of intermediate IEs is possible upon appropriate molecular scale mixing [114] (meant is mixing of different orientations of the same molecule, but the same argument holds for mixing of different molecules). Yet, a single molecule clearly has only one unique ionization energy irrespective of the orientation.

References

1. Jones, J. E. (1924). On the determination of molecular fields. II. From the equation of state of a gas. *Proceedings of the Royal Society of London. Series A*, *106*, 463–477.
2. Chelikowsky, J. R., & Cohen, M. L. (1974). Electronic structure of silicon. *Physical Review B*, *10*, 5095–5107.
3. Wang, D., Tang, L., Long, M., & Shuai, Z. (2009). First-principles investigation of organic semiconductors for thermoelectric applications. *The Journal of Chemical Physics*, *131*, 224704.
4. Hasegawa, T., & Takeya, J. (2009). Organic field-effect transistors using single crystals. *Science and Technology of Advanced Materials*, *10*, 024314.
5. Stillman, G., Wolfe, C., & Dimmock, J. (1970). Hall coefficient factor for polar mode scattering in n-type GaAs. *Journal of Physics and Chemistry of Solids*, *31*, 1199–1204.
6. Bässler, H. (1993). Charge Transport in disordered organic photoconductors a monte carlo simulation study. *Physica Status Solidi (b)*, *175*, 15–56.
7. Karl, N. (2003) Charge carrier transport in organic semiconductors. Synthetic Metals 133–134. In *Proceedings of the Yamada Conference LVI. The Fourth International Symposium on Crystalline Organic Metals, Superconductors and Ferromagnets (ISCOM 2001)* (pp. 649–657).
8. Holstein, T. (1959). Studies of polaron motion: Part I. The molecular-crystal model. *Annals of Physics*, *8*, 325–342.
9. Holstein, T. (1959). Studies of polaron motion: Part II. The small polaron. *Annals of Physics*, *8*, 343–389.
10. Yu, P. Y., & Cardona, M. (2010). *Fundamentals of Semiconductors* (4th ed.). Berlin: Springer.
11. Brütting, W., & Adachi, C. (2012). *Physics of Organic Semiconductors* (2nd ed.). John Wiley & Sons.
12. Czycholl, G. (2008). *Theoretische Festkörperphysik* (3rd ed.). Berlin: Springer.
13. Hückel, E. (1931). Quantentheoretische Beiträge zum Benzolproblem. *Zeitschrift für Physik*, *70*, 204–286.
14. Hückel, E. (1931). Quantentheoretische Beiträge zum Benzolproblem. *Zeitschrift für Physik*, *72*, 310–337.
15. Atkins, P. W., & Friedman, R. S. (1996). *Molecular Quantum Mechanics* (3rd ed.). Oxford University Press.
16. Atkins, P., & de Paula, J. (2006). *Physical Chemistry* (8th ed.). Oxford University Press.
17. Ashcroft, N. W., & Mermin, N. D. (1976) *Solid State Physics* (1st ed.). Harcourt College Publishers.

[14] Note that in the cited work push back occurs. Yet, what is important is that there is no interface dipole or Fermi–level pinning.

18. Garcia-Moliner, F., & Flores, F. (1976). Theory of electronic surface states in semiconductors. *Journal of Physics C: Solid State Physics*, *9*, 1609.
19. Heine, V. (1965). Theory of surface states. *Physical Review*, *138*, A1689–A1696.
20. Urbach, F. (1953). The long-wavelength edge of photographic sensitivity and of the electronic absorption of solids. *Physical Review*, *92*, 1324–1324.
21. John, S., Soukoulis, C., Cohen, M. H., & Economou, E. N. (1986). Theory of electron band tails and the urbach optical-absorption edge. *Physical Review Letters*, *57*, 1777–1780.
22. Boubaker, K. (2011). A physical explanation to the controversial Urbach tailing universality. *The European Physical Journal Plus*, *126*, 1–4.
23. Halperin, B. I., & Lax, M. (1966). Impurity-band tails in the high-density limit. I. Minimum counting methods. *Physical Review*, *148*, 722–740.
24. John, S., Chou, M. Y., Cohen, M. H., & Soukoulis, C. M. (1988). Density of states for an electron in a correlated Gaussian random potential: Theory of the Urbach tail. *Physical Review B*, *37*, 6963–6976.
25. Mott, N. (1967). Electrons in disordered structures. *Advances in Physics*, *16*, 49–144.
26. Tamm, I. (1932). On the possible bound states of electrons on a crystal surface. *Physikalische Zeitschrift der Sowjetunion*, *1*, 733.
27. Davison, S. G., & Steslicka, M. (1996) *Basic Theory of Surface States* (1st ed.). Clarendon Press.
28. Lüth, H. (1995). *Surfaces and Interfaces of Solid Materials* (3rd ed.). Berlin: Springer.
29. Stern, F. (1971). Band-tail model for optical absorption and for the mobility edge in amorphous silicon. *Physical Review B*, *3*, 2636–2645.
30. Morgan, T. N. (1965). Broadening of impurity bands in heavily doped semiconductors. *Physical Review*, *139*, A343–A348.
31. Cardy, J. L. (1978). Electron localisation in disordered systems and classical solutions in Ginzburg-Landau field theory. *Journal of Physics C: Solid State Physics*, *11*, L321.
32. John, S., & Stephen, M. J. (1984). Electronic density of states in a long-range correlated potential. *Journal of Physics C: Solid State Physics*, *17*, L559.
33. Soukoulis, C. M., Cohen, M. H., & Economou, E. N. (1984). Exponential band tails in random systems. *Physical Review Letters*, *53*, 616–619.
34. Anderson, P. W., Thouless, D. J., Abrahams, E., & Fisher, D. S. (1980). New method for a scaling theory of localization. *Physical Review B*, *22*, 3519–3526.
35. Soukoulis, C. M., & Economou, E. N. (1999). Electronic localization in disordered systems. *Waves in Random Media*, *9*, 255–269.
36. Redfield, D. (1975). Transport properties of electrons in energy band tails. *Advances in Physics*, *24*, 463–487.
37. Tiedje, T., Cebulka, J. M., Morel, D. L., & Abeles, B. (1981). Evidence for exponential band tails in amorphous silicon hydride. *Physical Review Letters*, *46*, 1425–1428.
38. Mirlin, A. D. (2000). Statistics of energy levels and eigenfunctions in disordered systems. *Physics Reports*, *326*, 259–382.
39. Lang, N. D., & Kohn, W. (1973). Theory of metal surfaces: induced surface charge and image potential. *Physical Review B*, *7*, 3541–3550.
40. Pierret, R. F. (2002). *Advanced Semiconductor Fundamentals* (2nd ed.). Prentice Hall.
41. Bierwagen, O., Ive, T., Walle, C. G. V. D. & Speck, J. S. (2008) Causes of incorrect carrier-type identification in van der Pauw-Hall measurements. *Applied Physics Letters*, *93*, 242108 (2008).
42. Look, D. C., et al. (2005). Evidence for native-defect donors in n-type ZnO. *Physical Review Letters*, *95*, 225502.
43. Shi, G. A., Saboktakin, M., Stavola, M., & Pearton, S. J. (2004). Hidden hydrogen in as-grown ZnO. *Applied Physics Letters*, *85*, 5601–5603.
44. Van de Walle, C. G. (2000). Hydrogen as a cause of doping in Zinc Oxide. *Physical Review Letters*, *85*, 1012–1015.
45. Lavrov, E. V., Weber, J., Börrnert, F., Van de Walle, C. G., & Helbig, R. (2002). Hydrogen-related defects in ZnO studied by infrared absorption spectroscopy. *Physical Review B*, *66*, 165205.

46. Lavrov, E. V., Herklotz, F., & Weber, J. (2009). Identification of hydrogen molecules in ZnO. *Physical Review Letters*, *102*, 185502.
47. Lavrov, E. V., Herklotz, F., & Weber, J. (2009). Identification of two hydrogen donors in ZnO. *Physical Review B*, *79*, 165210.
48. Allen, M. W., & Durbin, S. M. (2008). Influence of oxygen vacancies on Schottky contacts to ZnO. *Applied Physics Letters*, *92*, 122110.
49. Zhang, S. B., Wei, S.-H., & Zunger, A. (2001). Intrinsic n-type versus p-type doping asymmetry and the defect physics of ZnO. *Physical Review B*, *63*, 075205.
50. Qiu, H., Meyer, B., Wang, Y., & Wöll, C. (2008). Lonization energies of shallow donor states in ZnO created by reversible formation and depletion of H interstitials. *Physical Review Letters*, *101*, 236401.
51. Markevich, I. V., Kushnirenko, V. I., Borkovska, L. V., & Bulakh, B. M. (2005). Mechanism of formation of highly conductive layer on ZnO crystal surface. *Solid State Communications*, *136*, 475–478.
52. Ohgaki, T., et al. (2008). Positive Hall coefficients obtained from contact misplacement on evident n-type ZnO films and crystals. *Journal of Materials Research*, *23*, 2293–2295.
53. Look, D. C., Hemsky, J. W., & Sizelove, J. R. (1999). Residual native shallow donor in ZnO. *Physical Review Letters*, *82*, 2552–2555.
54. Kim, Y.-S., & Park, C. H. (2009). Rich variety of defects in ZnO via an attractive interaction between O vacancies and Zn interstitials: Origin of n-Type doping. *Physical Review Letters*, *102*, 086403.
55. Meyer, B. K., Sann, J., Hofmann, D. M., Neumann, C., & Zeuner, A. (2005). Shallow donors and acceptors in ZnO. *Semiconductor Science and Technology*, *20*, S62–S66.
56. Monakhov, E. V., Kuznetsov, A. Y., & Svensson, B. G. (2009). Zinc oxide: Bulk growth, role of hydrogen and Schottky diodes. *Journal of Physics D: Applied Physics*, *42*, 153001.
57. Oba, F., Nishitani, S. R., Isotani, S., Adachi, H., & Tanaka, I. (2001). Energetics of native defects in ZnO. *Journal of Applied Physics*, *90*, 824–828.
58. Janotti, A., & Van de Walle, C. G. (2007). Native point defects in ZnO. *Physical Review B*, *76*, 165202.
59. Park, C. H., Zhang, S. B., & Wei, S.-H. (2002). Origin of p-type doping difficulty in ZnO: The impurity perspective. *Physical Review B*, *66*, 073202.
60. Lyons, J. L., Janotti, A., & Van de Walle, C. G. (2009). Why nitrogen cannot lead to p-type conductivity in ZnO. *Applied Physics Letters*, *95*, 252105.
61. Lee, E.-C., Kim, Y.-S., Jin, Y.-G., & Chang, K. J. (2001). Compensation mechanism for N acceptors in ZnO. *Physical Review B*, *64*, 085120.
62. Look, D. C., et al. (2002). Characterization of homoepitaxial p-type ZnO grown by molecular beam epitaxy. *Applied Physics Letters*, *81*, 1830–1832.
63. Ryu, Y., et al. (2000). Synthesis of p-type ZnO films. *Journal of Crystal Growth*, *216*, 330–334.
64. Ryu, Y. R., Lee, T. S., & White, H. W. (2003). Properties of arsenic-doped p-type ZnO grown by hybrid beam deposition. *Applied Physics Letters*, *83*, 87–89.
65. Minegishi, K., et al. (1997). Growth of p-type zinc oxide films by chemical vapor deposition. *Japanese Journal of Applied Physics*, *36*, L1453–L1455.
66. Sze, S. M., & Ng, K. K. (2007). *Physics of semiconductor devices* (3rd edn). John Wiley & Sons Inc.
67. Traeger, F., Kauer, M., Wöll, C., Rogalla, D., & Becker, H.-W. (2011). Analysis of surface, subsurface, and bulk hydrogen in ZnO using nuclear reaction analysis. *Physical Review B*, *84*, 075462.
68. Koch, N. (2007). Organic electronic devices and their functional interfaces. *ChemPhysChem*, *8*, 1438–1455.
69. Hwang, J., Wan, A., & Kahn, A. (2009). Energetics of metal-organic interfaces: New experiments and assessment of the field. *Materials Science and Engineering: R*, *64*, 1–31.
70. Ishii, H., & Seki, K. (1997). Energy level alignment at organic/metal interfaces studied by UV photoemission: Breakdown of traditional assumption of a common vacuum level at the interface. *IEEE Transactions on Electron Devices*, *44*, 1295–1301.

71. Fukagawa, H., et al. (2007). The role of the ionization potential in vacuum-level alignment at organic semiconductor interfaces. *Advanced Materials*, *19*, 665–668.
72. Braun, S., Salaneck, W. R., & Fahlman, M. (2009). Energy-level alignment at organic/metal and organic/organic interfaces. *Advanced Materials*, *21*, 1450–1472.
73. Ishii, H., Sugiyama, K., Ito, E., & Seki, K. (1999). Energy level alignment and interfacial electronic structures at organic/metal and organic/organic interfaces. *Advanced Materials*, *11*, 605–625.
74. Wang, H., et al. (2014). Band-bending in organic semiconductors: The role of alkali-halide interlayers. *Advanced Materials*, *26*, 925–930.
75. Lange, I., et al. (2011). Band bending in conjugated polymer layers. *Physical Review Letters*, *106*, 216402.
76. Blakesley, J. C., & Greenham, N. C. (2009). Charge transfer at polymer-electrode interfaces: The effect of energetic disorder and thermal injection on band bending and open-circuit voltage. *Journal of Applied Physics*, *106*, 034507.
77. Nishi, T., Kanai, K., Ouchi, Y., Willis, M. R., & Seki, K. (2005). Evidence for the atmospheric p-type doping of titanyl phthalocyanine thin film by oxygen observed as the change of interfacial electronic structure. *Chemical Physics Letters*, *414*, 479–482.
78. Ishii, H. et al. (2004). Kelvin probe study of band bending at organic semiconductor/metal interfaces: Examination of Fermi level alignment. *Physica Status Solidi (a)*, *201*, 1075–1094.
79. Oehzelt, M., Koch, N., & Heimel, G. (2014). Organic semiconductor density of states controls the energy level alignment at electrode interfaces. *Nature Communications*, *5*, 4174.
80. Hu, Y., et al. (2009). Observation of a 2D electron gas and the tuning of the electrical conductance of ZnO nanowires by controllable surface band-bending. *Advanced Functional Materials*, *19*, 2380–2387.
81. Mönch, W. (1990). On the physics of metal-semiconductor interfaces. *Reports on Progress in Physics*, *53*, 221.
82. Vázquez, H., et al. (2004). Barrier formation at metal-organic interfaces: Dipole formation and the charge neutrality level. *Applied Surface Science*, *234*. *The Ninth International Conference on the Formation of Semiconductor Interfaces* (pp. 107–112).
83. Mönch, W. (2006). Slope parameters of the barrier heights of metal-organic contacts. *Applied Physics Letters*, *88*, 112116.
84. Cahen, D., & Kahn, A. (2003). Electron energetics at surfaces and interfaces: Concepts and experiments. *Advanced Materials*, *15*, 271–277.
85. Zhang, F., et al. (2007). Energy level alignment and morphology of interfaces between molecular and polymeric organic semiconductors. *Organic Electronics*, *8*, 606–614.
86. Hill, I. G., & Kahn, A. (1998). Energy level alignment at interfaces of organic semiconductor heterostructures. *Journal of Applied Physics*, *84*, 5583–5586.
87. Hill, I. G., & Kahn, A. (1999). Organic semiconductor heterointerfaces containing bathocuproine. *Journal of Applied Physics*, *86*, 4515–4519.
88. Braun, S., Osikowicz, W., Wang, Y., & Salaneck, W. R. (2007). Energy level alignment regimes at hybrid organic-organic and inorganic-organic interfaces. *Organic Electronics*, *8*, 14–20.
89. Bardeen, J. (1947). Surface states and rectification at a metal semi-conductor contact. *Physical Review*, *71*, 717–727.
90. Bredas, J. L., & Street, G. B. (1985). Polarons, bipolarons, and solitons in conducting polymers. *Accounts of Chemical Research*, *18*, 309–315.
91. Fahlman, M., et al. (2007). Electronic structure of hybrid interfaces for polymer-based electronics. *Journal of Physics: Condensed Matter*, *19*, 183202.
92. Winkler, S., et al. (2015) Probing the energy levels in hole-doped molecular semiconductors. *Materials Horizons* (2015).
93. Sueyoshi, T., Fukagawa, H., Ono, M., Kera, S., & Ueno, N. (2009). Low-density band-gap states in pentacene thin films probed with ultrahigh-sensitivity ultraviolet photoelectron spectroscopy. *Applied Physics Letters*, *95*, 183303.
94. Lang, N. D., & Kohn, W. (1970). Theory of metal surfaces: Charge density and surface energy. *Physical Review B*, *1*, 4555–4568.

95. Crispin, X., et al. (2002). Characterization of the interface dipole at organic/metal interfaces. *Journal of the American Chemical Society*, *124*, 8131–8141.
96. Hofmann, O. T., Rangger, G. M., & Zojer, E. (2008). Reducing the metalwork function beyond pauli pushback: A computational investigation of tetrathiafulvalene and viologen on coinage metal surfaces. *The Journal of Physical Chemistry C*, *112*, 20357–20365.
97. Lang, N. D. (1981). Interaction between closed-shell systems and metal surfaces. *Physical Review Letters*, *46*, 842–845.
98. Watkins, N. J., Yan, L., & Gao, Y. (2002). Electronic structure symmetry of interfaces between pentacene and metals. *Applied Physics Letters*, *80*, 4384–4386.
99. Schroeder, P. G., France, C. B., Park, J. B., & Parkinson, B. A. (2002). Energy level alignment and two-dimensional structure of pentacene on Au(111) surfaces. *Journal of Applied Physics*, *91*, 3010–3014.
100. Li, H., Duan, Y., Coropceanu, V., & Bredas, J.-L. (2009). Electronic structure of the pentacene-gold interface: A density-functional theory study. *Organic Electronics*, *10*, 1571–1578.
101. Greiner, M. T., et al. (2012). Universal energy-level alignment of molecules on metal oxides. *Nature Materials*, *11*, 76–81.
102. Winkler, S., et al. (2013). The impact of localwork function variations on fermi level pinning of organic semiconductors. *The Journal of Physical Chemistry C*, *117*, 22285–22289.
103. Witte, G., & Wöll, C. (2004). Growth of aromatic molecules on solid substrates for applications in organic electronics. *Journal of Materials Research*, *19*, 1889–1916.
104. Venables, J. A., Spiller, G. D. T., & Hanbucken, M. (1984). Nucleation and growth of thin films. *Reports on Progress in Physics*, *47*, 399.
105. Schreiber, F. (2004). Organic molecular beam deposition: Growth studies beyond the first monolayer. *Physica Status Solidi (a)*, *201*, 1037–1054.
106. Einax, M., Dieterich, W., & Maass, P. (2013). Colloquium: Cluster growth on surfaces: Densities, size distributions, and morphologies. *Reviews of Modern Physics*, *85*, 921–939.
107. Hlawacek, G., et al. (2008). Characterization of step-edge barriers in organic thin-film growth. *Science*, *321*, 108–111.
108. Ruiz, R., et al. (2003). Dynamic Scaling, island size distribution, and morphology in the aggregation regime of submonolayer pentacene films. *Physical Review Letters*, *91*, 136102.
109. Liu, H., Lin, Z., Zhigilei, L. V., & Reinke, P. (2008). Fractal structures in fullerene layers: Simulation of the growth process. *The Journal of Physical Chemistry C*, *112*, 4687–4695.
110. Evans, J., Thiel, P., & Bartelt, M. (2006). Morphological evolution during epitaxial thin film growth: Formation of 2D islands and 3D mounds. *Surface Science Reports*, *61*, 1–128.
111. Cox, E., et al. (2005). Temperature dependence of island growth shapes during submonolayer deposition of Ag on Ag(111). *Physical Review B*, *71*, 115414.
112. Smoluchowski, R. (1941). Anisotropy of the electronic work function of metals. *Physical Review*, *60*, 661–674.
113. Duhm, S., et al. (2008). Orientation-dependent ionization energies and interface dipoles in ordered molecular assemblies. *Nature Materials*, *7*, 326–332.
114. Salzmann, I., et al. (2008). Structural and electronic properties of pentacene-fullerene heterojunctions. *Journal of Applied Physics*, *104*(114518), 50.

http://www.springer.com/978-3-319-46623-1

Energy-Level Control at Hybrid Inorganic/Organic Semiconductor Interfaces

Schlesinger, R.

2017, XVIII, 211 p. 88 illus., 52 illus. in color., Hardcover
ISBN: 978-3-319-46623-1